

**AUGUST 2019**

**M.Sc. in Aircraft and Aerospace Engineering**

**MEHMET KIRMIZI**

**REPUBLIC OF TURKEY  
GAZIANTEP UNIVERSITY  
GRADUATE SCHOOL OF NATURAL & APPLIED SCIENCES**

**INVESTIGATING THE FLOW SEPERATION DUE TO  
GROOVES OVER A CYLINDRICAL SHAPE**

**M.Sc. THESIS  
IN  
AIRCRAFT AND AEROSPACE ENGINEERING**

**BY  
MEHMET KIRMIZI**

**AUGUST 2019**

**INVESTIGATING THE FLOW SEPARATION DUE TO  
GROOVES OVER A CYLINDRICAL SHAPE**

**M.Sc. Thesis**

**in**

**Aircraft and Aerospace Engineering  
Gaziantep University**

**Supervisor**

**Asst. Prof. Dr. Sohayb Abdul KARIM**

**Co-Supervisor**

**Asst. Prof. Dr. Erman ASLAN**

**by**

**Mehmet KIRMIZI**

**August 2019**



©2019[Mehmet KIRMIZI]

REPUBLIC OF TURKEY  
GAZIANTEP UNIVERSITY  
GRADUATE SCHOOL OF NATURAL & APPLIED SCIENCES  
AIRCRAFT AND AEROSPACE ENGINEERING

Name of the Thesis : Investigating the Flow Separation Due to Grooves Over a  
Cylindrical Shape

Name of the Student : Mehmet KIRMIZI

Exam Date : 29.08.2019

Approval of the Graduate School of Natural and Applied Sciences

Prof. Dr. A. Necmeddin YAZICI  
Director

I certify that this thesis satisfies all the requirements as a thesis for the degree of Master  
of Science.

Assoc. Prof. Dr. İbrahim GÖV  
Head of Department

This is to certify that we have read this thesis and that in our consensus/majority  
opinion it is fully adequate, in scope and quality, as a thesis for the degree of Master  
of Science.

Assist. Prof. Dr. Erman ASLAN  
Co-Supervisor

Assist. Prof. Dr. Sohayb Abdul KARIM  
Supervisor

Examining Committee Members:

Signature

Asst. Prof. Dr. Sohayb Abdul KARIM

.....

Assoc. Prof. Dr. İbrahim GÖV

.....

Asst. Prof. Dr. Jamal E. AFAGHANI

.....

**I hereby declare that all information in this document has been obtained and presented in accordance with academic rules and ethical conduct. I also declare that, as required by these rules and conduct, I have fully cited and referenced all material and results that are not original to this work.**

**Mehmet KIRMIZI**

## **ABSTRACT**

### **INVESTIGATING THE FLOW SEPERATION DUE TO GROOVES OVER A CYLINDRICAL SHAPE**

**KIRMIZI, Mehmet**

**M.Sc. in Aircraft and Aerospace Engineering**

**Supervisor: Asst. Prof. Dr. Sohayb Abdul KARIM**

**Co-Supervisor: Asst. Prof. Dr. Erman ASLAN**

**August 2019**

**50 pages**

Cylindrical objects are widely used in many engineering applications, especially in aerospace and aircraft engineering. In the present study, in an attempt to reduce the aerodynamic drag of a flow over a cylindrical shape, three cases of groove size were analyzed. For every case, the angular position of the groove was changed four times. The grooves were square-shaped and taken 5%, 10% and %15 of the cylinder diameters; while the angular positions were taken 30°, 45°, 60° and 75° relative to the forward stagnation point. The analysis was made numerically using finite volume method based on commercial code Ansys-Fluent. Bare (without grooves) circular cylinder was analyzed for the sake of validation at Re:10000. In order to perform a quantitative analysis, the drag coefficient, the RMS of lift coefficient and the Strouhal number were computed. Reynolds number was kept at 10000. Large Eddy Simulation (LES) method was applied for turbulence modelling. In the conclusion, it was found that two square grooves reduce the drag coefficient over cylinder.

**Key Words:** Circular Cylinder with Square Groove, Drag Coefficient, Large Eddy Simulations, Finite Volume Method, FLUENT.

## ÖZET

### AKIŞ AYRILMASININ SİLİNDİR ÜZERİNDEKİ ÇENTİKLER VASITASIYLA İNCELENMESİ

**KIRMIZI, Mehmet**

**Yüksek Lisans Tezi, Uçak ve Uzay Mühendisliği**  
**Danışmanı: Dr. Öğr. Üyesi Sohayp Abdul KARIM**  
**İkinci Danışmanı: Dr. Öğr. Üyesi Erman ASLAN**  
**Ağustos 2019**  
**50 sayfa**

Silindirik cisimler başta uçak ve uzay mühendisliği olmak üzere birçok mühendislik uygulamasında yaygın olarak kullanılmaktadır. Bu çalışmada, silindirik cisimde üç farklı boyutlu çentik kullanılarak sürüklenme katsayısının düşürülmesi amaçlandı. Her çentik boyutu için, çentiklerin açıl pozisyonları dört kez değiştirildi. Çentikler karesel şekilli olup boyutları silindir çapının %5, %10 ve % 15'i kadarken, açıl pozisyonları ön durgunluk noktasına göre 30°, 45°, 60° ve 75°dir. Analizler sayısal olarak sonlu hacim tabanlı açık kodlu Ansys-Fluent programı kullanılarak yapıldı. Reynolds sayısı 10.000'de doğrulama için çentiksiz silindir analizi yapıldı. Nicel bir analiz olması için sürüklenme katsayısı, taşıma katsayısının R.M.S'i ve Strouhal sayısı hesaplandı. Bütün analizler için Reynolds sayısı 10.000 olarak belirlendi. Türbülans modeli olarak büyük girdap simülasyonu (LES) modeli kullanıldı. Sonuç olarak iki kare çentik kullanmanın sürüklenme katsayısını düşürdüğü görüldü.

**Anahtar Kelimeler:** Kare Çentikli Silindir, Sürüklenme Katsayısı, Büyük Girdap Simülasyonu, Sonlu Hacim Yöntemi, FLUENT

## **ACKNOWLEDGEMENTS**

Firstly, I am very grateful to my supervisor Assist. Prof. Dr. Sohayp Abdul Karim and my Co-supervisor Assist. Prof. Dr. Erman Aslan for their guidance and support from the beginning to the end of this study. It has been an honor to be their student as well. Without their guidance and persistent help this dissertation would not have been possible.

I would like to thank to, my friends instructor Ali Biçer, instructor Fatih Arslan and Eng. Ahmet Ekmen for their valuable comments and moral support.

The deepest thankfulness is to my parents, brothers and sisters, for their endless support and interest.



## TABLE OF CONTENTS

<b>ABSTRACT</b> .....	<b>vii</b>
<b>ÖZET</b> .....	<b>viii</b>
<b>ACKNOWLEDGEMENTS</b> .....	<b>vii</b>
<b>TABLE OF CONTENTS</b> .....	<b>viii</b>
<b>LIST OF TABLES</b> .....	<b>xi</b>
<b>LIST OF FIGURES</b> .....	<b>xi</b>
<b>LIST OF SYMBOLS</b> .....	<b>xivv</b>
<b>CHAPTER 1</b> .....	<b>1</b>
<b>INTRODUCTION</b> .....	<b>1</b>
1.1 General Introduction.....	1
1.2 Research Objectives .....	1
1.3 Layout of Thesis .....	2
<b>CHAPTER 2</b> .....	<b>3</b>
<b>LITERATURE SURVEY</b> .....	<b>3</b>
2.1 Introduction .....	3
2.2 Flow Regime for Cylinder.....	3
2.3 Drag .....	6
2.4 Lift .....	6
2.5 The Strouhal Number .....	7
2.6 Vortex Shedding.....	7
2.7 Active Flow Control Methods .....	8
2.8 Passive Flow Control Methods.....	9
<b>CHAPTER 3</b> .....	<b>13</b>

<b>NUMERICAL MODEL AND FORMULATION .....</b>	<b>13</b>
3.1 Governing equation .....	13
3.1.1 Continuity equation.....	13
3.1.2 Navier-stokes Equation.....	13
3.2 Computational Fluid Dynamic .....	13
3.3 Turbulence Modeling .....	14
3.3.1 Large Eddy Simulation (LES) .....	15
3.4 Ansys-Fluent .....	15
3.5 Modeling and Simulation Procedure .....	15
3.5.1 Geometry and Boundary Condition.....	16
3.6 Meshing .....	18
3.7 Initialization and Solving the Model .....	21
<b>CHAPTER 4 .....</b>	<b>22</b>
<b>RESULT AND DISCUSSION.....</b>	<b>22</b>
4.1 Flow Around Bare Circular Cylinder .....	22
4.2 Analysis of drag, Clrms and Strouhal number for 0.05D.....	25
4.3 Analysis of drag, Clrms and Strouhal number for 0.1D.....	32
4.4 Analysis of drag, Clrms and Strouhal number for 0.15D.....	39
<b>CHAPTER 5 .....</b>	<b>46</b>
<b>CONCLUSION.....</b>	<b>46</b>
<b>REFERENCES.....</b>	<b>48</b>

## LIST OF TABLES

	<b>Page</b>
<b>Table 2.1</b> Flow regions around circular cylinders .....	5
<b>Table 3.1</b> The used number of meshes .....	21
<b>Table 4.1</b> Compared to experimental and present numerical data for bare cylinder.....	23
<b>Table 4.2</b> The length of $L_R$ , a and b for bare cylinder .....	23
<b>Table 4.3</b> Strouhal number, drag coefficient and root mean square of lift coefficient values for bare cylinder and different angular positions of grooves cylinder .....	25
<b>Table 4.4</b> The length of $L_R$ , a and b for 0.05D .....	26
<b>Table 4.5</b> Strouhal number, drag coefficient and root mean square of lift coefficient values for bare cylinder and different angular positions of grooves cylinder .....	32
<b>Table 4.6</b> The length of $L_R$ , a and b for 0.1D .....	34
<b>Table 4.7</b> Strouhal number, drag coefficient and root mean square of lift coefficient values for bare cylinder and different angular positions of grooves cylinder .....	39
<b>Table 4.8</b> The length of $L_R$ , a and b for 0.1D .....	41

## LIST OF FIGURES

	<b>Page</b>
<b>Figure 2.1</b> Vortex shedding in the wake region of the flow past a circular cylinder (Dyke, 1982).....	8
<b>Figure 3.1</b> The schematic figure for flow past a cylinder .....	17
<b>Figure 3.2</b> The computational domain with boundaries .....	17
<b>Figure 3.3</b> Groove sizes and angular positions .....	18
<b>Figure 3.4</b> Two-dimensional meshes for smooth cylinder.....	19
<b>Figure 3.5</b> Three-dimensional mesh details for smooth cylinder .....	19
<b>Figure 3.6</b> Two-dimensional mesh for 0.05D grooved size cylinder .....	20
<b>Figure 3.7</b> Three-dimensional mesh for 0.05D grooved size at cylinder wall.....	20
<b>Figure 4.1</b> A sketch of the time-averaged flow structure around a circular cylinder (Zhou et al., 2015) .....	23
<b>Figure 4.2</b> Instantaneous x velocity contour for bare cylinder at Re:10.000.....	24
<b>Figure 4.3</b> Mean x velocity contour for bare cylinder at Re:10.000 .....	24
<b>Figure 4.4</b> The time-averaged streamlines for bare cylinder .....	24
<b>Figure 4.5</b> Instantaneous streamlines for bare cylinder .....	24
<b>Figure 4.6</b> Variation of drag coefficient with angular positions for 0.05D .....	25
<b>Figure 4.7</b> Variation of root mean square of lift coefficient with angles for 0.05D. ....	26

<b>Figure 4.8</b>	The time-averaged streamlines for (a) 0.05D - 30°, (b) 0.05D - 45°, (c) 0.05D - 60°, (d) 0.05D - 75° and (e) bare circular cylinder .....	28
<b>Figure 4.9</b>	The instantaneous streamlines for (a) 0.05D - 30°, (b) 0.05D - 45°, (c) 0.05D - 60°, (d) 0.05D - 75° and (e) bare circular cylinder .....	29
<b>Figure 4.10</b>	The mean x velocity contour for (a) 0.05D - 30°, (b) 0.05D - 45°, (c) 0.05D - 60°, (d) 0.05D - 75° and (e) bare circular cylinder .....	30
<b>Figure 4.11</b>	The instantaneous x velocity contour for (a) 0.05D - 30°, (b) 0.05D - 45°, (c) 0.05D - 60°, (d) 0.05D - 75° and (e) bare circular cylinder .....	31
<b>Figure 4.12</b>	Variation of drag coefficient with angular positions for 0.1D .....	33
<b>Figure 4.13</b>	Variation of root mean square of lift coefficient with angles for 0.1D. ....	33
<b>Figure 4.14</b>	the time-averaged streamlines for (a) 0.1D - 30°, (b) 0.1D - 45°, (c) 0.1D - 60°, (d) 0.1D - 75° and (e) bare circular cylinder .....	35
<b>Figure 4.15</b>	The instantaneous streamlines for (a) 0.1D - 30°, (b) 0.1D - 45°, (c) 0.1D - 60°, (d) 0.1D - 75° and (e) bare circular cylinder .....	36
<b>Figure 4.16</b>	The mean x velocity contour for (a) 0.1D - 30°, (b) 0.1D - 45°, (c) 0.1D - 60°, (d) 0.1D - 75° and (e) bare circular cylinder .....	37
<b>Figure 4.17</b>	The instantaneous x velocity contour for (a) 0.1D - 30°, (b) 0.1D - 45°, (c) 0.1D - 60°, (d) 0.1D - 75° and (e) bare circular cylinder .....	38
<b>Figure 4.18</b>	Variation of drag coefficient with angles for 0.15D .....	40
<b>Figure 4.19</b>	Variation of root mean square of lift coefficient with angles for 0.15D. ....	40
<b>Figure 4.20</b>	The time-averaged streamlines for (a) 0.15D - 30°, (b) 0.15D - 45°, (c) 0.15D - 60°, (d) 0.15D - 75° and (e) bare circular cylinder .....	42

**Figure 4.21** The instantaneous streamlines for (a) 0.15D - 30°, (b) 0.15D - 45°, (c) 0.15D - 60°, (d) 0.15D - 75° and (e) bare circular cylinder ..... 43

**Figure 4.22** The mean x velocity contour for (a) 0.15D - 30°, (b) 0.15D - 45°, (c) 0.15D - 60°, (d) 0.15D - 75° and (e) bare circular cylinder ..... 44

**Figure 4.23** The instantaneous x velocity contour for (a) 0.15D - 30°, (b) 0.15D - 45°, (c) 0.15D - 60°, (d) 0.15D - 75° and (e) bare circular cylinder ..... 45



## LIST OF SYMBOLS

$\mu$	Dynamic viscosity (kg/m s)
<b>A</b>	Area (m <sup>2</sup> )
<b>C<sub>D</sub></b>	Drag coefficient
<b>CFD</b>	Computational Fluid Dynamic
<b>D</b>	Diameter of cylinder (m)
<b>DES</b>	Detached Eddy Simulation
<b>DNS</b>	Direct Numerical Simulation
<b>F</b>	Force (N)
<b>F<sub>D</sub></b>	Drag force
<b>f<sub>s</sub></b>	Frequency of Lift Coefficient
<b>LES</b>	Large Eddy Simulation
<b>DES</b>	Detached Eddy Simulation
<b>NS</b>	Navier-Stokes
<b>PISO</b>	Pressure Implicit with Splitting Operators
<b>RANS</b>	Reynolds Averaged Navier-Stocks
<b>Re</b>	Reynolds number
<b>RKE</b>	Realizable K-Epsilon
<b>SIMPLE</b>	Semi-Implicit Method for Pressure-Linked Equations

<b>SIMPLEC</b>	SIMPLE Corrected/Consistent
<b>SKE</b>	Standard K-Epsilon
<b>SST</b>	Shear Stress Transport
<b>St</b>	Strouhal number
<b>U</b>	Local velocity (m/s)
<b>V</b>	Velocities (m/s)
<b><math>\theta</math></b>	Angular Position of Grooves
<b><math>\rho</math></b>	Density (kg/m <sup>3</sup> )
<b><math>\nu</math></b>	Kinematic viscosity



## CHAPTER 1

### INTRODUCTION

#### 1.1 General Introduction

Investigation of flow around bluff bodies were object of curiosity for researchers. These studies are date back till 1900s. Understanding flow around bluff bodies has been a prominent topic due to fluid-structure interaction term. If a bluff body is immersed in a flow domain, periodically vortices shedding from the upper and lower surfaces led to the vibrations of structural. Under certain cases, these vibrations would cause to structural damages that may be disastrous, as in the even that resonance. Therefore, the flow control for circular cylinder is crucial. There are two type of flow control for cylinder. These are active and passive flow control methods. The active flow control methods include feedback control, electromagnetic control, rotating circular cylinder, wake heating, suction and blowing. The passive flow control methods include such as splitter plate, base bleed, surface protrusion, surface groove and dimples. Passive flow control methods are preferred because of they are simpler and cheaper than active flow control methods.

Computational Fluid Dynamics is a beneficial instrument for illustrate the flow field via velocity vectors, streamlines, contours lines, etc. for miscellaneous flow conditions. The lift and drag coefficient, pressure coefficient, Strouhal number, fluctuating of lift and forces exerted on the structures can also be determined by using the CFD techniques. Investigation of the flow behind a cylinder at Reynolds numbers 10000 is done in the present study. The numerical analyses were performed by employing the LES turbulence model and the finite volume based commercial code ANSYS FLUENT.

#### 1.2 Research Objectives

Using many grooves on the surface of the cylinder can have adverse effect such as decreasing strength and extra drag force. Main purpose of this thesis is to find proper groove configuration in order to control flow at Reynolds number 10000. In order to

determine the most proper groove configuration, different configurations were tested. In the present study, in an attempt to reduce the aerodynamic drag of a flow over a cylindrical shape, two cases of groove size were analyzed. The fundamental objective of this thesis has to determine the proper configuration and sizes of grooves for decreasing drag force at circular cylinder.

### **1.3 Layout of Thesis**

Introduction and general information about the flow during circular cylinders, and the aims of the thesis are presented in Chapter 1. A literature review about passive and active flow control for cylinder, flow regime, vortex shedding, and aerodynamic force has been summarized in Chapter 2. An over view of Computational Fluid Dynamics (CFD), turbulence, turbulence models in CFD, LES, creation of the geometry and the boundary conditions, meshing, simulation, the numerical model set-up, specification of boundary conditions, initialization and solving the model, are given in Chapter 3. Results and discussions are also interpreted about all of cases grooved circular cylinder chapter 4. In the Chapter 5, conclusion has been given.

## CHAPTER 2

### LITERATURE SURVEY

#### 2.1 Introduction

Investigation of flow behind circular cylindrical shapes has been studied by many researchers in different engineering applications such as marine, civil, aircraft and aerospace. There are two types of flow control methods for cylinder. These are active flow control and passive flow control methods. Therefore, literature divided by two as active control methods and passive control methods. These studies were carried out as experimentally and numerically.

#### 2.2 Flow Regime for Cylinder

The non-dimensional aerodynamic parameters describing the flow past circular cylinders rely on the Reynolds number ( $Re$ ). Irish scientist Osborne Reynolds defined Reynolds number and give his name. It is given by below:

$$Re = \frac{V \cdot D}{\nu} = \frac{\rho \cdot V \cdot D}{\mu} = \frac{\text{Inertial force}}{\text{Viscous force}}$$






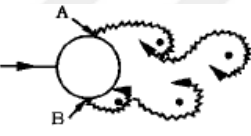
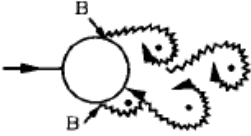


where  $V$  (m/s) is the flow velocity,  $D$  (m) is the diameter of the cylinder,  $\nu$  is the Kinematic viscosity,  $\rho$  ( $\text{kg/m}^3$ ) is density and  $\mu$  ( $\text{kg/m.s}$ ) is the dynamic viscosity. Velocity fluctuation, spectra, and frequency of flow regimes for miscellaneous Reynolds numbers were first off described by Roshko (Roshko 1954). There are several flow regimes from creeping flows to entirely turbulent flows for circular cylinder and they can be classified as below:

The flow is two-dimensional and steady with just two separation points, which is at the beginning and at the end of the cylinder, at  $Re < 5$ . With the range  $5 < Re < 40$ , again the flow is still two-dimensional and steady, but a vortex pair exists past the circular cylinder, whose length of recirculation zone increases linearly with Reynolds number (Bathcelor, 1967).

When the  $Re$  is enhanced to the critical the Reynolds numbers, the wake becomes unstable and the periodic vortex shedding phenomenon occurs behind the cylinder. Vortex is shed alternately on both side of the circular cylinder at a dependent frequency. Therefore, the wake has the appearances of the vortex street. Again, the shedding is actually two-dimensional, but it is unsteady (Williamson, 1989).

The region of the transition to turbulence pulls away from the cylinder as the Reynolds is raise in the range  $200 < Re < 300$ . Bloor reported in a study that the vortices formed are turbulent at  $Re = 400$  (Bloor, 1964). Other Researchers declared that the two-dimensional character of the vortex shedding found in the range of  $40 < Re < 200$ , become openly three-dimensional in the identical range (General, 1978 and Williamson, 1988). Shed of vortices take placed in cells in the spanwise direction of the flow. The Reynolds number range of  $300 < 3 \times 10^5$  has been called the subcritical range, since it happens prior to the onset of the turbulent boundary layer at Reynolds number of nearly  $3 \times 10^5$ .

**Table 2.1** Flow regions behind circular cylinders (Sumer B.M. and Fredsøe J. 1997)

	Non- separation and Creeping flow	Re less than 5 ( $Re < 5$ )
	A fixed pair of symmetric vortices	$5 < Re < 40$
	Laminar vortex street (Periodic)	$40 < Re < 200$
	Transition to turbulence in the wake region	$200 < Re < 300$
	Entirely turbulent in wake. A. Boundary layer separation is laminar	$300 < Re < 3 \times 10^5$ Subcritical
	A. Separation laminar boundary layer. B. Laminar at boundary layer but separation at turbulent boundary layer	$2 \times 10^5 < Re < 3.5 \times 10^5$ Critical (Lower transition)
	B. Separation at turbulent boundary layer, and boundary layer partially laminar partially turbulent.	$3.5 \times 10^5 < Re < 1.5 \times 10^6$ Supercritical
	C. Entirely turbulent at one side in boundary layer.	$1.5 \times 10^6 < Re < 4 \times 10^6$ Upper transition
	C. Entirely turbulent at both sides in boundary layer.	$4 \times 10^6 < Re$ Transcritical

In the range of  $3 \times 10^5 < Re < 3.5 \times 10^5$  as illustrated in Table 2.1, the boundary layer becomes turbulent at the separation point, on the other hand this occurs only at one phase of the circular cylinder. That flow regime is recognized as the critical regime (Sumer B.M. and Fredsøe J. 2006).

As known Supercritical flow regime is a range of  $3.5 \times 10^5$  to  $1.5 \times 10^6$ . The turbulent boundary layer separation occurs in this region at top of and the bottom sides of the circular cylinder. Nevertheless, transition to turbulence in the boundary layers has not been still performed. Transition to turbulent regime is seated somewhere between the separation point and the stagnation point. As known upper-transition flow regime in the range of  $1.5 \times 10^6 < Re < 4.5 \times 10^6$  is illustrated in table 2.1. It is fully turbulent occurring from the boundary layer on one side and partly turbulent on the other side of the circular cylinder. Finally, for  $Re > 4.5 \times 10^6$  the boundary layer over the plane of cylinder called the transcritical flow regime which is an entirely turbulent flow everywhere.

### 2.3 Drag

Drag is an aerodynamic force and is created by contact of a solid body with a fluid. The drag force depends on Reynolds number and it is used as a non-dimensionalized form which name is drag coefficient. The drag force enhances with enhances in air velocity and in diameter of the cylinder. The boundary layer separation occurs at approximately  $82^\circ$  and  $140^\circ$  from the stagnation point for laminar and turbulent flow conditions, respectively. After separation point the pressure coefficient remains negative total pressure drag.

The total pressure drag on the circular cylinder is calculated by given formula;

$$C_D = \frac{F_D}{0.5\rho u_0^2 A}$$

where  $F_D$  is drag force,  $\rho$  is density,  $u_0$  is velocity, and  $A$  is planform area.

### 2.4 Lift

Lift is an aerodynamic force in the direction normal to uniform flow. It is formed by the interaction and contact of a solid body with a fluid.

Lift is also used as a non-dimensional form, namely lift coefficient. Lift depends on the fluid's velocity, the fluid's viscosity, the density of the fluid and compressibility, the geometric shape of the object, the surface area over which the fluids, flows, and the body's inclination to the flow like the drag force.

$$C_L = \frac{F_L}{0.5\rho u_0^2 A}$$

where  $\rho$  is density,  $u_0$  is velocity,  $A$  is planform area and  $F_L$  is lift force. R.M.S of lift coefficient is calculated as;

$$rms_{lift-coefficient} = \sqrt{\frac{(C_{L,1}^2 + C_{L,2}^2 + \dots + C_{L,n}^2)}{n}}$$

where  $n$  is the iteration number.

## 2.5 The Strouhal Number

The Strouhal number puts forward a measure of the rate of the inertial forces on account of the unsteadiness of the flow or local acceleration to the inertial forces on account of alters in velocity from one point to another in the flow domain. The Strouhal number of a stationary tube is generally depend on Reynolds number, it is less function of surface roughness and freestream turbulence.

The Strouhal number can be expressed as;

$$St = \frac{fD}{u_0}$$

where  $D$  is diameter of cylinder,  $u_0$  is velocity and  $f$  is frequency of lift coefficient.

## 2.6 Vortex Shedding

Vortex shedding occurs when a fluid hits a solid body, which is caused alternating vortices to form at a specific frequency. The vortices conceive at fallen pressure regions on the downwind side of the body. Vortices produce a vibration at a specific computable frequency. Sumer and Fredsoe had described the theory of vortex shedding phenomena (Sumer and Fredsoe, 1997). Figure 2.1 is presented vortex shedding in the wake region of the flow behind a circular cylinder.



**Figure 2.1** Vortex shedding in the wake region of the flow past a circular cylinder (Dyke, 1982)

## **2.7 Active Flow Control Methods**

Active control methods have been improved to apply some types of energy into the flow for control of vortex shedding. The purpose of active control is to use the instability of the wake, to implicitly change drag and the mean wake velocity profile. The instability of the wake causes the vortices. Electro-magnetic control, rotating circular cylinder, wake heating, feedback control, suction and blowing are primary kind of active flow control methods.

Active control methods have been improved to apply some types of energy into the flow for control of vortex shedding. The velocity field were measured with using Particle image velocimetry (PIV) technique for each system. They observed that oscillatory motion of a circular cylinder to be an efficient method for controlling the near-wake flow structure (Lee et al, 2007).

Yuan and Cheng studied experimentally the high frequency perturbation effects on the performance of depressing-flow induced vibration (FIV). They revealed that the probability to depress both structural vibration and wake vortex by introducing a perturbation input at a high-frequency range well-exceeding resonant frequency of structure (Yuan and Cheng, 2007).

The electromagnetic force to control the flow past a circular cylinder was introduced by Kim and Lee. They used to active flow control method called electromagnetic control. The aim of this study investigated the impact of the electromagnetic force on



the cross-flow of a cylinder by establishing electrodes and stable magnets side by side alternately in the axial direction of the circular cylinder (Kim and Lee, 2000).

Feng et al fulfill to investigate control the flow behind a cylinder using a synthetic jet positioned at the rear stagnation point with a novel synthetic jet. They used to active flow control method called suction and blowing. Their study showed that, when enhanced the suction duty cycle factor, the momentum coefficient is also enhanced, and a stronger and larger scale synthetic jet vortex pair is created, and it can get at further downstream. This characteristic has a profound effect on the wake vortex shedding of the cylinder (Feng et al., 2010).

The flow past a circular cylinder with the aid of a control algorithm using multiple-feedback sensors and actuators was performed numerically investigated by Muddada and Patnaik (2009). They used to active flow control method called acoustic excitation. They revealed that the rate of steady state injection bases on the proportionality coefficient, that is to say lower the rate of injection, the slower it will reach steady state and viceversa.

## **2.8 Passive Flow Control Methods**

Passive control purposes perturbation of the flow structure modifications on the blunt body or with placing external parts into the downstream of the flow. Passive control techniques contain geometric shaping to manipulate the aerodynamic forces, the use of fixed vortex generators for boundary layer separation control. Passive control techniques are widely used for flow control applications. There are many passive control methods surface protrusion (tripping wire, fin, helical strakes, helical wires, studs, grooved cylinder, etc.), shrouds (perforated gauze, axial rods, etc.), near-wake stabilizers (splitter plate, guiding plate, base-bleed, slits cut along the models, etc.). The passive control techniques have advantages of simplified construction and no additional power input.

Flow around a finite and an infinite circular cylinder with specific height-to-diameter ratio is performed by Zhang et al. with using large eddy simulation. The used ratio is 1.5. Only one Reynolds number ( $Re=3900$ ) is defined. It is observed that finite cylinder produces less drag coefficient than infinite cylinder, the decreasing ratio is

approximately 25%. At the same time reduction of the fluctuating lift coefficient was 60% for finite circular cylinder as compared to the infinite one (Zhang et al., 2013).

Dong and Karniadakis investigated flow behind oscillating and stationary circular cylinder at Reynold number 10000 using (direct numerical simulation) DNS. With significant increasing Reynolds number, multilevel-type parallel algorithm within the spectral element framework is used for DNS. The conclusion of their research shows that, the drag coefficients, lift coefficients and the Strouhal number are close to the experimental results. Oscillating frequency of cylinders alters from 0.14 to 0.25. In this range, the drag coefficient varies slightly while the lift Coefficient enhances significantly as the oscillation frequency enhances. The conclusion of their study illustrated that, results of DNS is close the available experimental data (Dong and Karniadakis, 2005).

Khashehchi et al investigated experimental flow characteristic for foamed and finned circular cylinders at the wide range of Reynold numbers from 1000 to 10000. The experimental study was performed in low speed wind tunnel. They calculated and compared mean velocity, instantaneous velocity and instantaneous vorticity for bare, finned and foamed circular cylinder. The conclusions of this research showed that the dimension of the flow structure increases when fins or foam are mounted to the cylinder affecting the flow pattern on the behind circular cylinder (Khashehchi et al., 2014).

Owen et al. studied experimentally for measuring the drag and vortex-induced vibration amplitudes of a cylinder. They used a circular cross- sectional body with a sinuous axis and a circular cylinder with hemispheric lumps attached. Their study mentioned drag reductions of nearly 25% and suppression of vortex shedding for the circular cylinder with lumps (Owen et al., 2001).

Karabelas et al. investigated the flow past a rotating circular cylinder using 2D  $k-\varepsilon$  turbulence model at high Reynolds number. Their study examined the effect of spin ratio on the load exerted by the fluid over a cylinder. 12 rotational rates from 0 to 8 were determined, at three different Reynold numbers such  $5 \times 10^5$ ,  $10^6$  and  $5 \times 10^6$ . This research shows that the lift and drag coefficient change less than 10% in the Reynolds

numbers range. Drag force increases up to spin ratio  $a=4$  and then decreases. However, lift force increases linearly with spin ratio (Karabelas et al., 2012).

The experimental research of flow over circular cylinder via a longitudinally grooved was performed by Zhou et al. The study's purpose understanding the effect of a grooved surface on the drag coefficient. In this study was used 16 uniform rectangular longitudinal grooves at circular cylinder. They carried out to measurement the drag force at four different Reynold Number range from  $7.4 \times 10^3$  to  $1.8 \times 10^4$ . Additionally, turbulent kinetic energy, distributions of the mean velocities and Reynolds normal stress were gotten by using particle image velocimetry (PIV) technique. Usage wavy surfaces reduced the mean drag coefficient approximately %20 with the reference of bare cylinder. For better comparison, the same Reynolds number are used (Zhou et al., 2015a).

The experimental investigation of flow around cylinder with bare, grooved and dimpled was performed by Zhou et al. This study's purpose understanding the effect of rough surface on the drag coefficient. They carried out to measurement the drag force at four different Reynold Number range from  $7.4 \times 10^3$  to  $1.8 \times 10^4$  and distributions of the time averaged velocities, Reynolds stress were get by using PIV technique. The result of study reveals that the grooved and dimpled circular cylinders decrease mean drag coefficient. Specifically, the mean reduction of dimpled circular cylinder is from 10% to 30%, while the grooved circular cylinder is ranged from 18% to 29%. The result of PIV shows that the dimpled or grooved surface roughness reduces the cylinder recirculation zone in terms of the the streamwise position, recirculation length and the transverse spacing of the primary eddies (Zhou et al., 2015b).

Liu et al made an experimental study for investigating the influence of a splitter plate on the wake flow cylinder. The control elements of the splitter plate length,  $L/D$  was changed from 0 to 1.5 and the Reynolds number determined at 2400 and 3000. The PIV measurement was carried out to indicate wake flow structures. The result of experimental study showed that the splitter plate length and Reynold number as significant control parameters had influence on wake flow structures (Liu et al., 2016).

Kim et al performed study related to the influence of Reynolds number turbulent near wake behind cylinder using Large eddy simulation turbulence method. The Reynolds number was determined as 5500 and 41300. The present study obviously revealed that the overall patterns and locations of the peak values of the mean flow statistics moved upstream near to the circular cylinder base with increasing Reynolds number (Kim et al., 2014).

Canpolat investigated flow behind a cylinder with a groove, using particle image velocimetry technique at Reynolds number 5000. Six different rectangular groove sizes were determined for different angular positions ( $0^\circ \leq \theta \leq 150^\circ$ ). It was observed that, using of groove on a cylinder surface remarkably affects the near wake flow structure and turbulence statics. (Canpolat, 2015) Another experimental study which using PIV, is made by Canpolat and Sahin (2017). Effect of passive flow control mechanism of single groove on a circular cylinder surface was presented in that study. It is observed that,  $\theta = 80^\circ$  is the critical angular position of groove. It means flow separation starts at  $\theta = 80^\circ$ . The flow separation is controlled within  $0^\circ \leq \theta \leq 80^\circ$ .

## CHAPTER 3

### NUMERICAL MODEL AND FORMULATION

#### 3.1 Governing Equation

Continuity equation and Navier-Stokes (N-S) are used as the governing equations for the 3D turbulent incompressible flow around the bare and grooved circular cylinder at subcritical Reynolds Numbers 10.000.

##### 3.1.1 Continuity Equation

The continuity equation depends on the principles of conservation of mass. Incompressible fluids, the amount of fluid entering and leaving the system is assumed constant. The equation of continuity expresses called conservation of mass. The equation of continuity given below.

$$\frac{\partial u_x}{\partial x} + \frac{\partial u_y}{\partial y} + \frac{\partial u_z}{\partial z} = 0$$

In the incompressible flow, the density ( $\rho$ ) is considered constant. Therefore, in the continuity equation, the change in density over time is zero.

##### 3.1.2 Navier-stokes Equation

The Navier-Stokes equations of incompressible fluids are the fundamental partial differentials equations and given by

$$\rho \left( \frac{\partial u_x}{\partial t} + u_x \frac{\partial u_x}{\partial x} + u_y \frac{\partial u_x}{\partial y} + u_z \frac{\partial u_x}{\partial z} \right) = -\frac{\partial P}{\partial x} + \eta \left( \frac{\partial^2 u_x}{\partial x^2} + \frac{\partial^2 u_x}{\partial y^2} + \frac{\partial^2 u_x}{\partial z^2} \right) + F_x$$

$$\rho \left( \frac{\partial u_y}{\partial t} + u_x \frac{\partial u_y}{\partial x} + u_y \frac{\partial u_y}{\partial y} + u_z \frac{\partial u_y}{\partial z} \right) = -\frac{\partial P}{\partial y} + \eta \left( \frac{\partial^2 u_y}{\partial x^2} + \frac{\partial^2 u_y}{\partial y^2} + \frac{\partial^2 u_y}{\partial z^2} \right) + F_y$$

$$\rho \left( \frac{\partial u_z}{\partial t} + u_x \frac{\partial u_z}{\partial x} + u_y \frac{\partial u_z}{\partial y} + u_z \frac{\partial u_z}{\partial z} \right) = -\frac{\partial P}{\partial z} + \eta \left( \frac{\partial^2 u_z}{\partial x^2} + \frac{\partial^2 u_z}{\partial y^2} + \frac{\partial^2 u_z}{\partial z^2} \right) + F_z$$

$F_x, F_y, F_z$  are body forces

The Navier-Stokes equations for incompressible flow can be dimensionless formulated with the substitutions of  $x, y, z, u, p$  and  $t$  expressed in:

$$X = \frac{x}{L}$$

$$Y = \frac{y}{L}$$

$$Z = \frac{z}{L}$$

$$U_x = \frac{u}{U_\infty}$$

$$P' = \frac{p-p_\infty}{0,5\rho U^2}$$

$$T = \frac{t}{L/U_\infty}$$

And  $F_x, F_y, F_z$  are zero

For X- Direction

$$\frac{\partial U_x}{\partial T} + U_x \frac{\partial U_x}{\partial X} + U_y \frac{\partial U_x}{\partial Y} + U_z \frac{\partial U_x}{\partial Z} = -\frac{\partial P'}{\partial X} + \frac{1}{Re} \left( \frac{\partial^2 U_x}{\partial X^2} + \frac{\partial^2 U_x}{\partial Y^2} + \frac{\partial^2 U_x}{\partial Z^2} \right)$$

For the Directions in Y and Z can be expressed in an analogous manner.

### 3.2 Computational Fluid Dynamic

The conservation equations for momentum, energy, mass and flow geometry are for CFD Solving relevantly. Flows and associated phenomena can be defined by partial differential equations, which are in many cases immensely difficult to solve analytically due to the non-linear inertial terms. To obtain correct results the domain in which the partial differential equations are defined, has to be discretized using sufficiently little grids. Hence, correctness of the numerical solution is related to the quality of discretization used (Fergizer and Peric, 1996).

### 3.3 Turbulence Modeling

Turbulent modelling is the establishment and usage of a model to predict the impact of turbulence. Averaging is frequently used to facilitate the solution of the governing equations of turbulent, however models are required to symbolize scales of the flow

that are not resolved. It is used for all types of turbulence models such as standard  $k-\epsilon$ , Realizable  $k-\epsilon$ , Wilcox  $k-\omega$ , SST  $k-\omega$ , Reynolds stress model, Spalart – All Maras model, detached eddy simulation models (DES) and large eddy simulation (LES) (Chen and Jaw, 1998).

### **3.3.1 Large Eddy Simulation (LES)**

LES is an unsteady formulation and offer fine results for all flow systems. The model is depended on Navier–Stokes equations and calculate large-scale turbulent fluctuations and models only the tiny scale fluctuations. Because it is a transient formulation, the required more time for calculation than the other models. Moreover, a finer mesh is looked for to achieve the most benefit from the LES model and to completely capture the turbulence in the smallest, subgrid scale eddies. In present study using LES as turbulence model. The Large Eddy Simulation are applied in this study for the turbulence modelling. The LES model has been developed by Smagorinsky (Smagorinsky, 1963).

### **3.4 Ansys-Fluent**

ANSYS FLUENT is an appropriate Computational Fluid Dynamic (CFD) software. ANSYS is used to simulate interaction of all soft practice of physics, structural mechanics, fluid dynamics, and vibration, electromagnetic and heat transfer. It is used for all types of turbulence models such as standard  $k-\epsilon$ , Realizable  $k-\epsilon$ , Wilcox  $k-\omega$ , SST  $k-\omega$ , Reynolds stress model, Spalart – Allmaras model, large eddy simulation (LES) and detached eddy simulation models (DES). ANSYS FLUENT is a commercial code which has high-performance computing capabilities and can model two-dimensional and three-dimensional structures capable of flows of turbulent, transient, laminar, incompressible, compressible, and steady behaviors. The ANSYS 17.0 version is used in present study.

### **3.5 Modeling and Simulation Procedure**

Numerical simulation of flow behind cylinder have been studied by various software, for example ANSYS-FLUENT, Abaqus/Cfd, Star-Ccm+ and Comsol. A number of these computer programs are commercially available and well known. In this study ANSYS-FLUENT version 17.0 is performed on two cores, with 12 CPU's (totally 24 CPU's) which is Intel (R) Xeon (R) CPU e5-2630 V2 2.60GHz. Also, this Dell

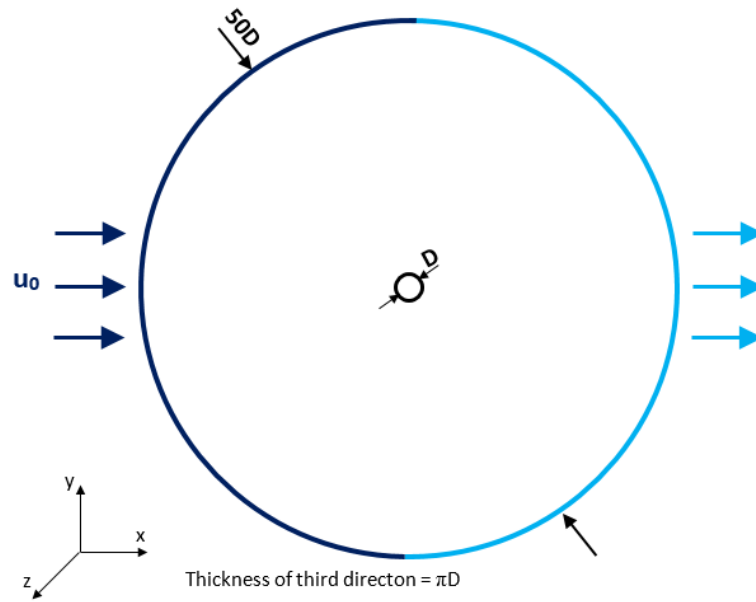
workstation has 24GB RAM. ANSYS is used to simulate interaction of all soft practice of physics, structural mechanics, fluid dynamics, and vibration, electromagnetic and heat transfer. It is used for all types of turbulence models such as standard k- $\epsilon$ , Realizable k- $\epsilon$ , Wilcox k- $\omega$ , SST k- $\omega$ , Reynolds stress model, Spalart – Allmaras model, detached eddy simulation models (DES) and large eddy simulation (LES).

The continuity equations coupled with the time-dependended incompressible Navier-Stokes equations and LES turbulence model equation are solved using the finite volume method based commercial, multi-purpose CFD code Ansys-Fluent (2009). The Large Eddy Simulation are applied in this study for the turbulence modelling. The LES model has been developed by Smagorinsky (1963). In the LES model, the large-scale motions are explicitly computed whereas the small edies are modelled. Smagorinsky-Lilly is used as a subgrid-scale model, and  $C_s=0.1$  is taken as model constant. The applied turbulence model equations are capable of representing the near wall turbulence, provided that the grid resolution is sufficiently fine.

### **3.5.1 Geometry and Boundary Condition**

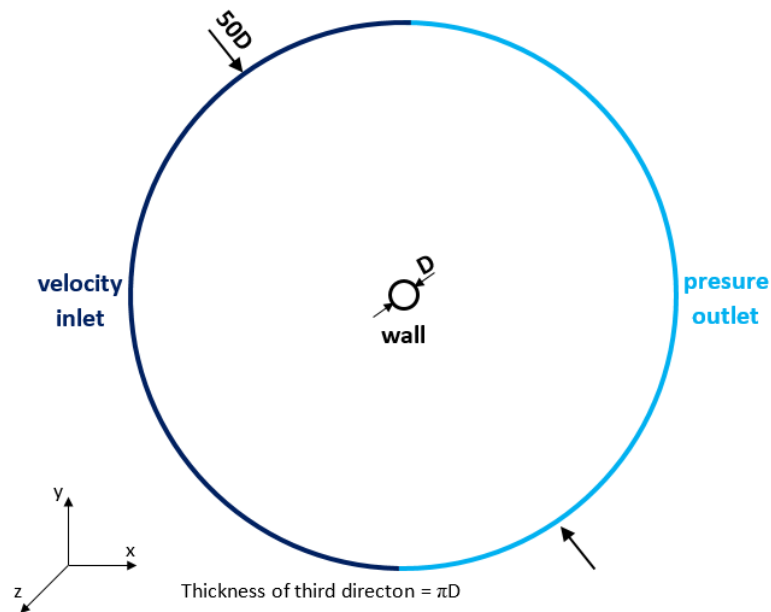
The geometry was created using GAMBIT software what is used to create geometry and meshing software. The computational domain for the simulation of the flow behind smooth and grooved cylinder is illustrated in Figure 3.1. The length of diameter was determined 0.01m (D) for the smooth and grooved circular cylinders. The length of diameter was determined 0.5 m (50D) for outer, and the thickness of flow domain is  $\pi.D$ .





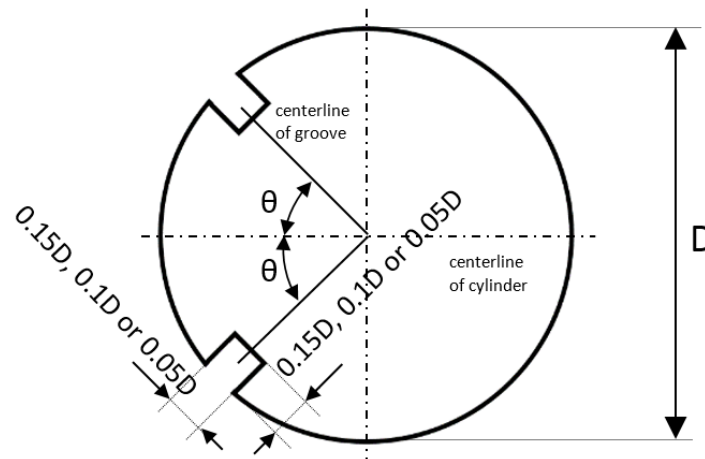
**Figure 3.1** The schematic figure computational domain for flow behind cylinder

Figure 3.2 shows the computational domain with specified boundaries. At the inlet was applied the velocity inlet as boundary condition. X-component velocity was settled at the velocity inlet boundary condition. At the outlet was imposed pressure outlet as boundary condition. No-slip boundary conditions are set at walls.



**Figure 3.2** The computational domain with boundaries

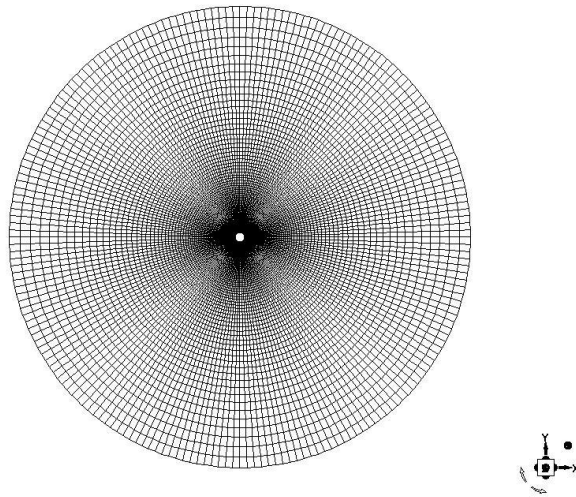
In this study used to two square shaped grooves for investigation flow past a circular cylinder. Three different groove sizes and four different angular position are determined for this study. The grooves were square-shaped and taken 5%, 10% and 15% of the cylinder diameters; while the angular positions were taken 30, 45°, 60° and 75° relative to the forward stagnation point.



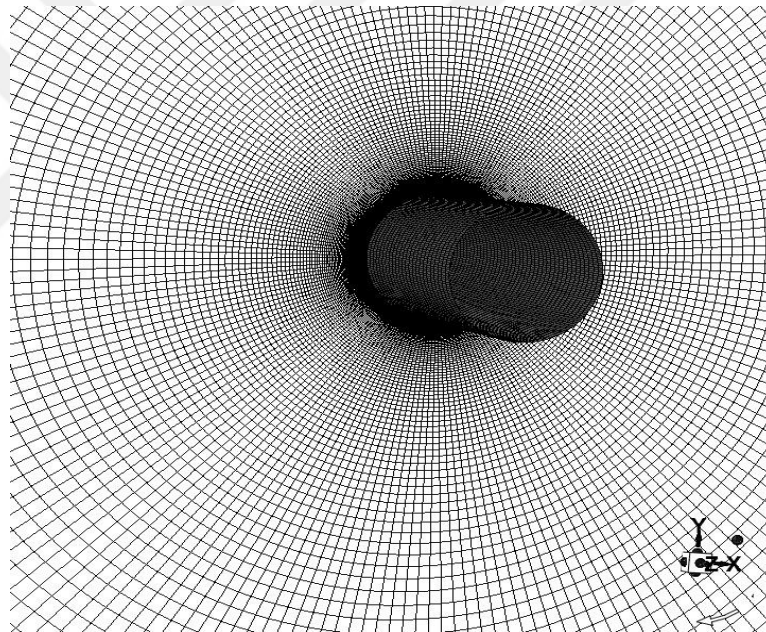
**Figure 3.3** Groove sizes and angular positions

### 3.6 Meshing

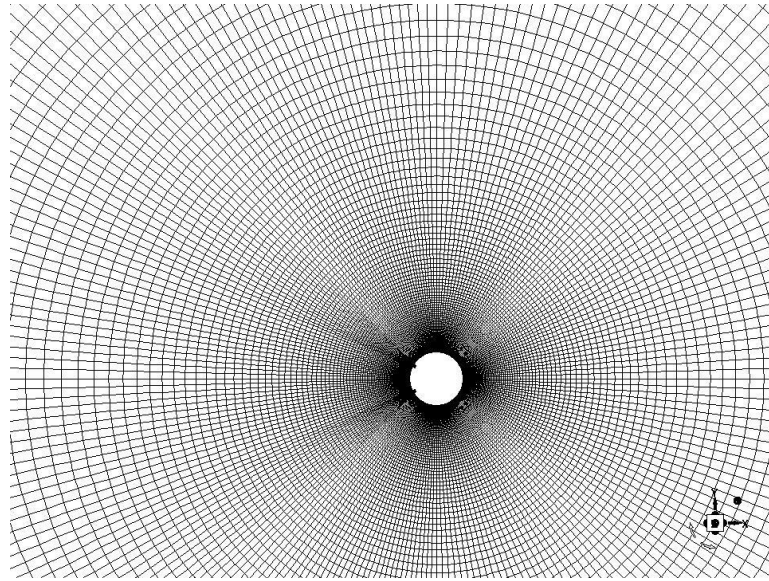
The mesh was created using GAMBIT software what is used to create geometry and meshing software Three-dimensional meshes are created by sweeping a two-dimensional mesh in the spanwise direction. For the purpose of the three-dimensional numerical computations, structured mesh strategy are used for discretizations. Two-dimensional meshes and three-dimensional mesh details for smooth cylinder are presented in figure 3.4 and figure 3.5, respectively. Two-dimensional meshes and three-dimensional mesh on the cylinder wall for 0.05D grooved size cylinder are presented in figure 3.6 and figure 3.7, respectively.



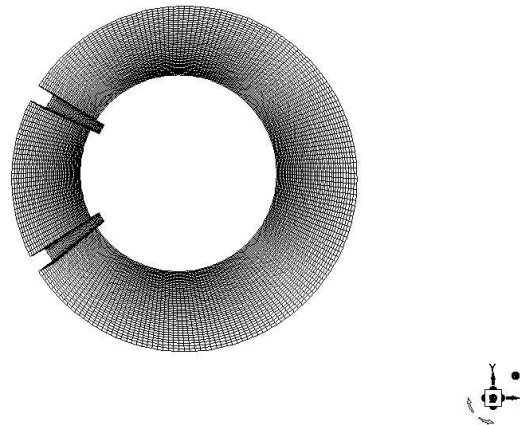
**Figure 3.4** Two-dimensional meshes for smooth cylinder



**Figure3.5** Three-dimensional mesh details for smooth cylinder



**Figure 3.6** Two-dimensional mesh for 0.05D grooved size cylinder



**Figure 3.7** Three-dimensional mesh for 0.05D grooved size at cylinder wall

A formal grid independent study was not carried out. For determining mesh resolutions, the previous experience of other authors (Benim et al. (2008)) is utilized. They used at least 200 cells to discretize the circumference of circular cylinder, which is also accepted in the present thesis. 48 cells are used in third direction. For modelling the near-wall turbulence, there is no usage wall functions. It is ensured that the distance of first near-wall cell fulfill the condition of  $y^+ < 1$ . In unsteady calculations, time step size has been chosen in a such a way that the cell Courant number takes a value about unity. The used number of meshes are shown in Table 3.1.

**Table 3.1.** The used number of meshes

Groove size	0.05D	0.15D	0.15D
30°	1 936 704	1 994 480	2 141 760
45°	1 936 704	1 994 480	2 141 760
60°	1 936 704	1 994 480	2 141 760
75°	1 936 704	1 994 480	2 141 760
Bare cylinder		1 680 000	

### 3.7 Initialization and Solving the Model

The velocity inlet at the x-direction is introduced as (14.61m/s). Reynolds numbers 10000. The density of fluid and the temperature are given  $1.225 \text{ kg/m}^3$  and  $288^\circ \text{ K}$ , respectively. At the outlet is imposed pressure outlet as boundary condition. No-slip boundary condition is applied at walls. In unsteady calculations, time step size has been chosen in a such a way that the cell Courant number takes a value about unity. The data sampling time has selected to  $200D/U$  for bare and grooved circular cylinders.

In order to make spatial discretization, Least Square Cell Based, PRESTO and Bounded Central Differencing are used for gradient, pressure and momentum, respectively. A second-order implicit scheme is used for integration in time. PISO algorithm is used for pressure-velocity coupling. Default underrelaxation factors (momentum: 0.7, pressure: 0.3). The residual value  $10^{-6}$  is required for all equations as the convergence criteria.

## CHAPTER 4

### RESULT AND DISCUSSION

#### 4.1 Flow Around Bare Circular Cylinder

Investigation of recirculation length, drag coefficient, rms of lift coefficient and Strouhal number is done numerically for bare cylinder and cylinder with two grooves for  $Re=10000$  with using finite volume based commercial code Ansys-Fluent. Bare (without grooves) circular cylinder was analyzed for the sake of validation at  $Re:10000$ . In order to perform a quantitative analysis, the drag coefficient, the RMS of lift coefficient, the Strouhal number were computed for bare circular cylinder. As a result of the analysis, Strouhal number and drag coefficient were found to be consistent with experimental literature. Zhou et al. carried out measurement of the drag force at four different Reynolds Number range from  $7.4 \times 10^3$  to  $1.8 \times 10^4$ . When interpolated, this drag coefficient is estimated to be 1.08 for Reynolds numbers 10000. The drag coefficient was computed 1.02 which value is consistent with Zhou et al.'s study. Figure 4.2 and Figure 4.3 indicate instantaneous and mean velocity contours for bare cylinder, respectively.

The recirculation zone is observed after the cylinders, whereas the maximum velocities are acquired at the top and the bottom of the cylinder. Length of recirculation zone is an important parameter for understanding flow mechanism.

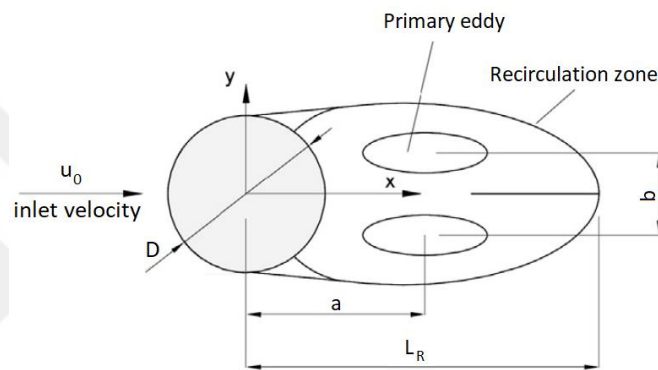
Strouhal number was calculated as 0.209 which value is in good agreement with the experimental data (Norberg, 2003).

**Table 4.1** Compared to experimental and present numerical data for bare cylinder

Case	St	$C_d$
Norberg (2003)	0.202	-
Zhou et al. (2015)	-	1.08
Present study	0.209	1.02

As shown in the table 4.1, drag coefficient and Strouhal number were found close to the experimental data for bare circular cylinder. Thus, the data for the cylinder was verified.

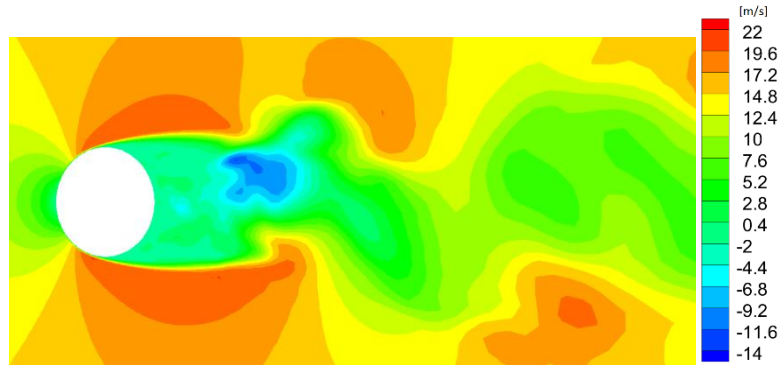
Figure 4.1 shows time-averaged flow structure around circular cylinder. A symmetrical recirculation zone with primary eddy is presented about longitudinal axis. Recirculation length ( $L_R$ ) is measured form the center of cylinder in the streamwise direction  $x$ . The notation  $a$  denotes to the length between cylinder center and primary eddy center from their streamwise position. Additionally,  $b$  presents the length between center of two primary eddies in cross-stream direction.



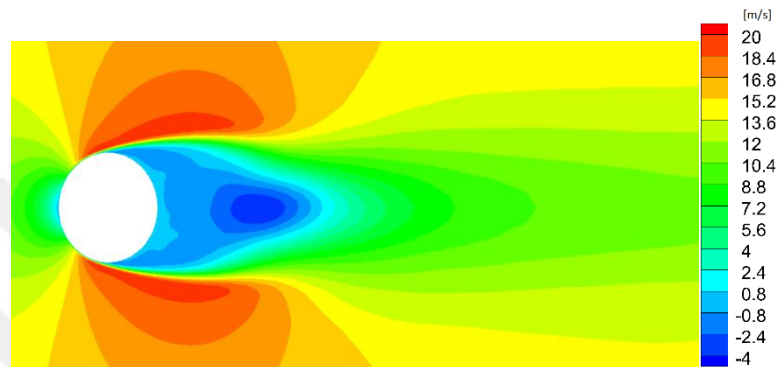
**Figure 4.1** A sketch of the time-averaged flow structure around a circular cylinder (Zhou et al., 2015)

**Table 4.2.** The length of  $L_R$ ,  $a$  and  $b$  for bare cylinder

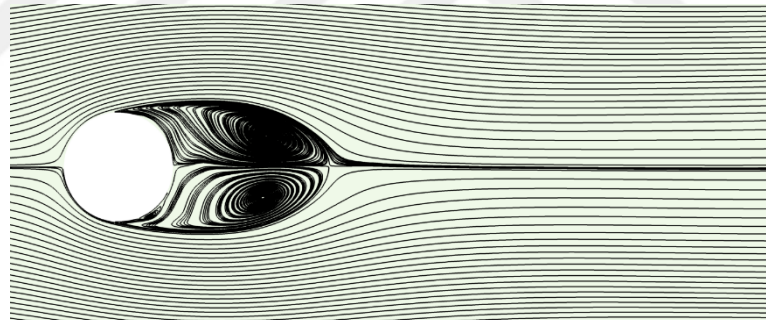
	$L_R$	$a$	$b$
Bare cylinder	1.98D	1.34D	0.55D



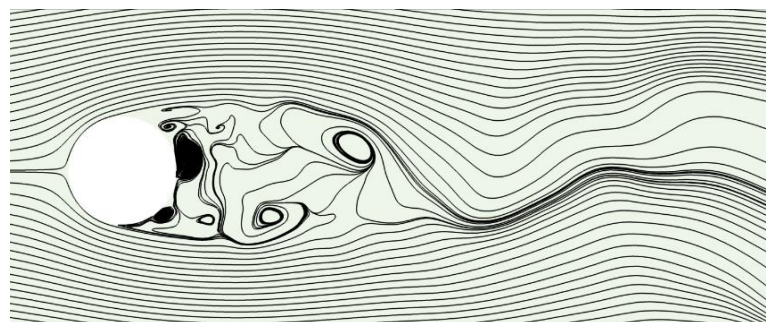
**Figure 4.2** Instantaneous x velocity contour for bare cylinder at Re:10.000



**Figure 4.3** Mean x velocity contour for bare cylinder at Re:10.000



**Figure 4.4** The time-averaged streamlines for bare cylinder



**Figure 4.5** Instantaneous streamlines for bare cylinder



## 4.2 Analysis of drag, $C_{lrms}$ and Strouhal number for 0.05D

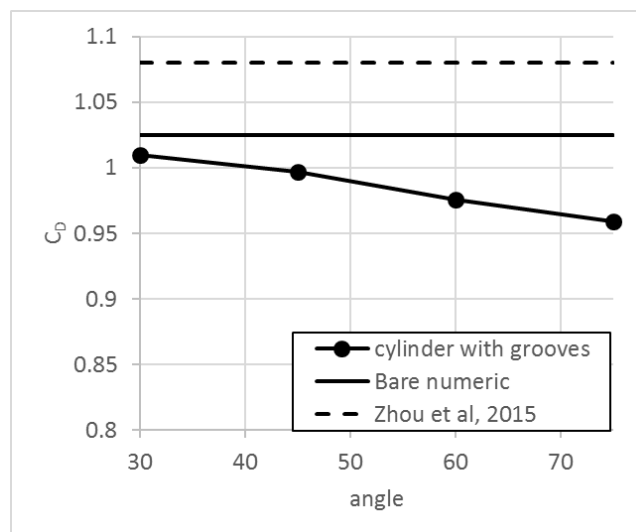
In this section, we will discuss the simulation for 0.05D grooves size cylinder. The angular position of the groove was changed four times. The grooves were square-shaped and taken 5% of the cylinder diameters; while the angular positions were taken 30°, 45°, 60° and 75° relative to the forward stagnation point.

As shown in the table 4.3, drag coefficient, Strouhal number and R.M.S of lift coefficient for different angular position grooves cylinder were compared with bare circular cylinder. As it can be seen in table 4.3 Strouhal number has not changed with angular position. That is shown, 0.05 D size of grooves have not affected unsteadiness of the flow past a circular cylinder.

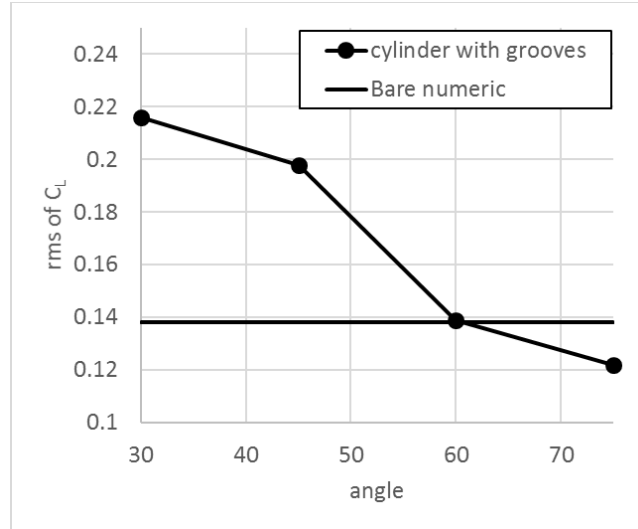
**Table 4.3** Strouhal number, drag coefficient and R.M.S of lift coefficient values for bare cylinder and different angular positions of grooves cylinder

Case	St	$C_d$	$C_{lrms}$
0.05D-30°	0.209	1.01	0.216
0.05D-45°	0.209	0.99	0.198
0.05D-60°	0.209	0.97	0.139
0.05D-75°	0.209	0.95	0.122
Bare cylinder	0.209	1.02	0.139

The drag coefficient 30° 0.05D groove sized circular cylinder is slightly lower than the drag coefficient bare circular cylinder. The drag coefficient for 45°, 60°, 75° angular position grooved cylinder is lower than bare cylinder. Variation of drag coefficient with angular positions for 0.05D is shown in Figure 4.6.



**Figure 4.6** Variation of drag coefficient with angular positions for 0.05D



**Figure 4.7** Variation of R.M.S of lift coefficient with angles for 0.05D.

Figure 4.7 shows the variation of rms of lift coefficient with angles for 0.05D. R.M.S of lift coefficient is smaller than bare cylinder for 0.05D and 75°, but R.M.S of lift for other cases of 0.05D groove sized cylinders are generally bigger than the bare cylinder.

**Table 4.4** The length of  $L_R$ ,  $a$  and  $b$  for 0.05D

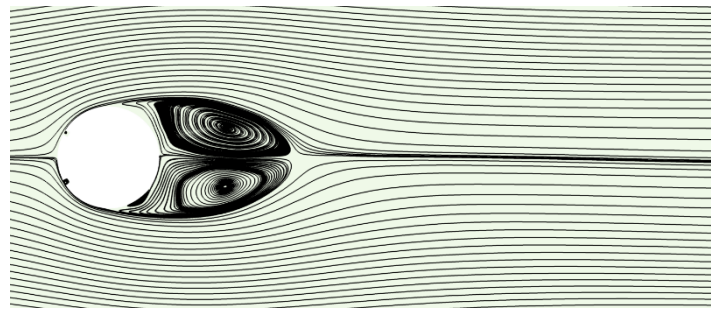
	$L_R$	$a$	$b$
0.05D- 30°	2.08D	1.14D	0.57D
0.05D- 45°	1.88D	1.28D	0.55D
0.05D- 60°	1.95D	1.375D	0.425D
0.05D- 75°	2.00D	1.33D	0.60D
bare cylinder	1.98D	1.34D	0.55D

Figure 4.8 presents the time-averaged streamlines for (a) 0.05D - 30°, (b) 0.05D - 45°, (c) 0.05D - 60°, (d) 0.05D - 75° and (e) bare circular cylinder. For better comparison, the nondimensional stream function has been used, the minimum and maximum nondimensional stream function values are “0” and “1”, respectively. The step size between streamlines is 0.004. After the cylinder, the recirculation zone and primary eddy is shown clearly for all cases. The length of  $L_R$ ,  $a$  and  $b$  are given at Table 4.4 for all cases of 0.05D. Figure 4.9 presents the instantaneous streamlines for (a) 0.05D - 30°, (b) 0.05D - 45°, (c) 0.05D - 60°, (d) 0.05D - 75° and (e) bare circular cylinder. The instantaneous velocity distributions are not symmetric for all cases.

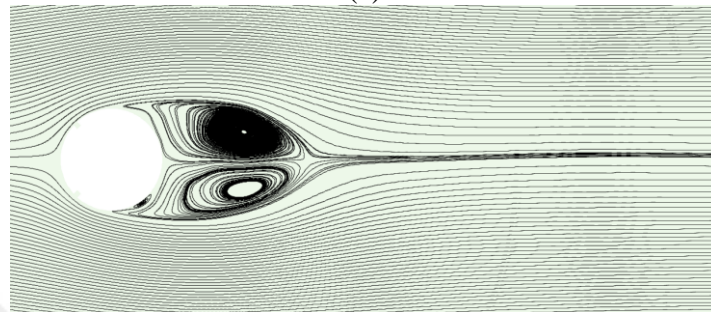
Figure 4.10 shows the time-averaged x-velocity distributions for for (a) 0.05D - 30°, (b) 0.05D - 45°, (c) 0.05D - 60°, (d) 0.05D - 75° and (e) bare circular cylinder. The time of 200D/U is taken for averaging of time. The recirculation zone is observed after

the cylinders, whereas the maximum velocities are acquired at top of and the bottom the cylinder for all cases. Length of recirculation zone is important parameter for understanding flow mechanism. Figure 4.11 shows instantaneous x velocity contour for for (a)  $0.05D - 30^\circ$ , (b)  $0.05D - 45^\circ$ , (c)  $0.05D - 60^\circ$ , (d)  $0.05D - 75^\circ$  and (e) bare circular cylinder. The instantaneous velocity distributions are not enough to have knowledge about flow structure, whereas the maximum velocities are acquired at top of and the bottom cylinder for all cases.

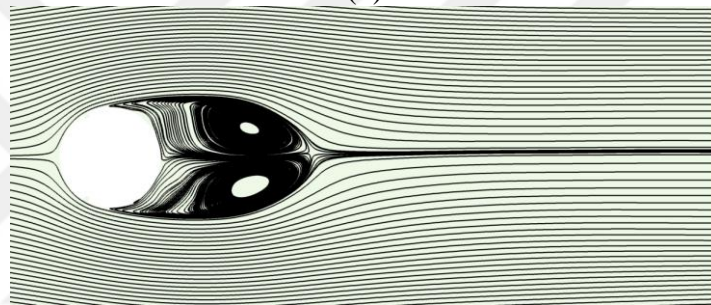




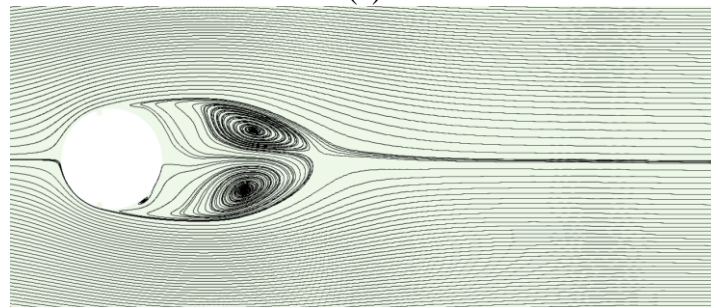
(a)



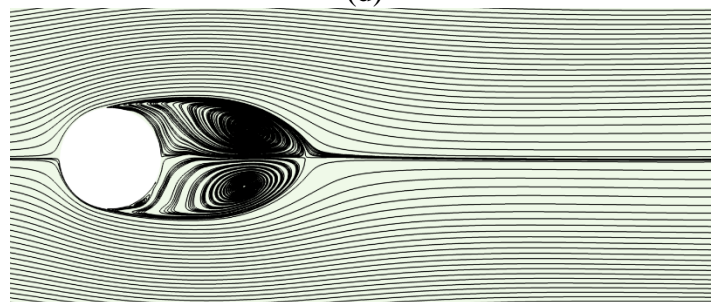
(b)



(c)

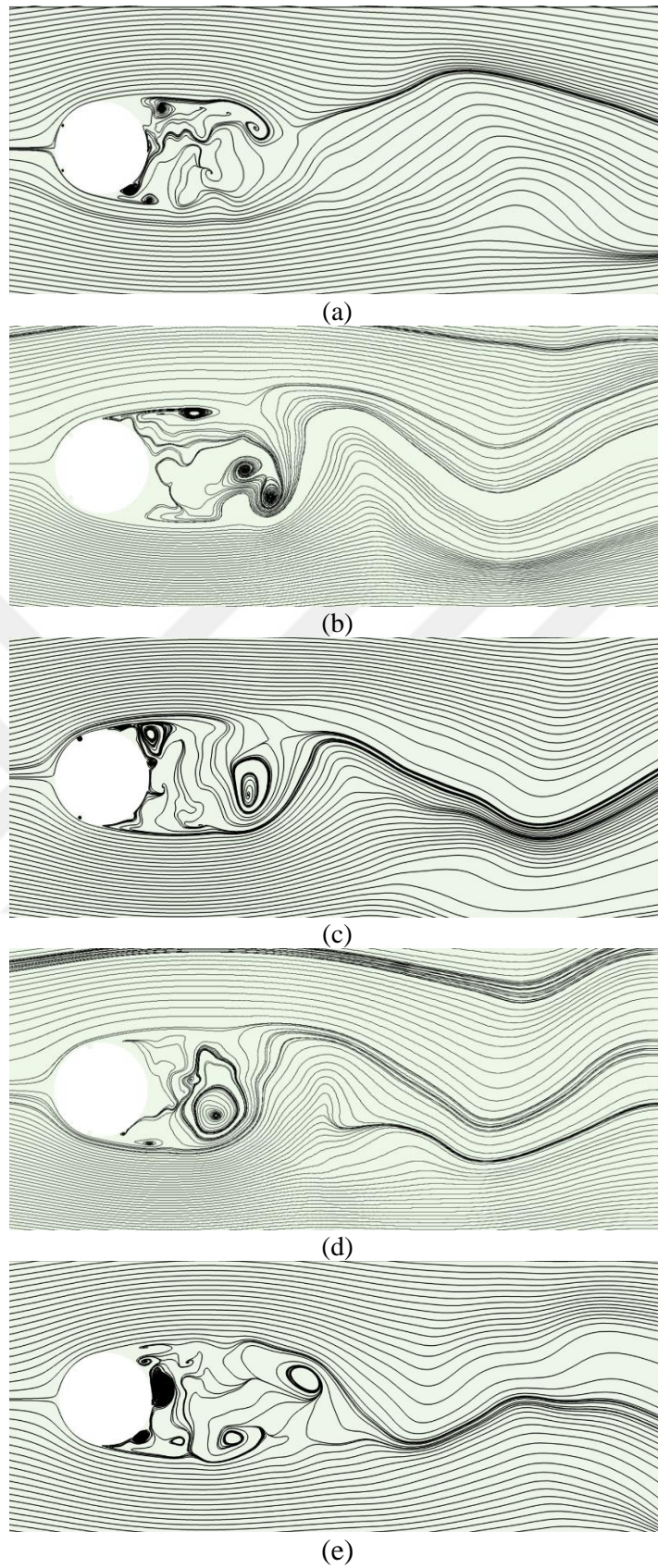


(d)

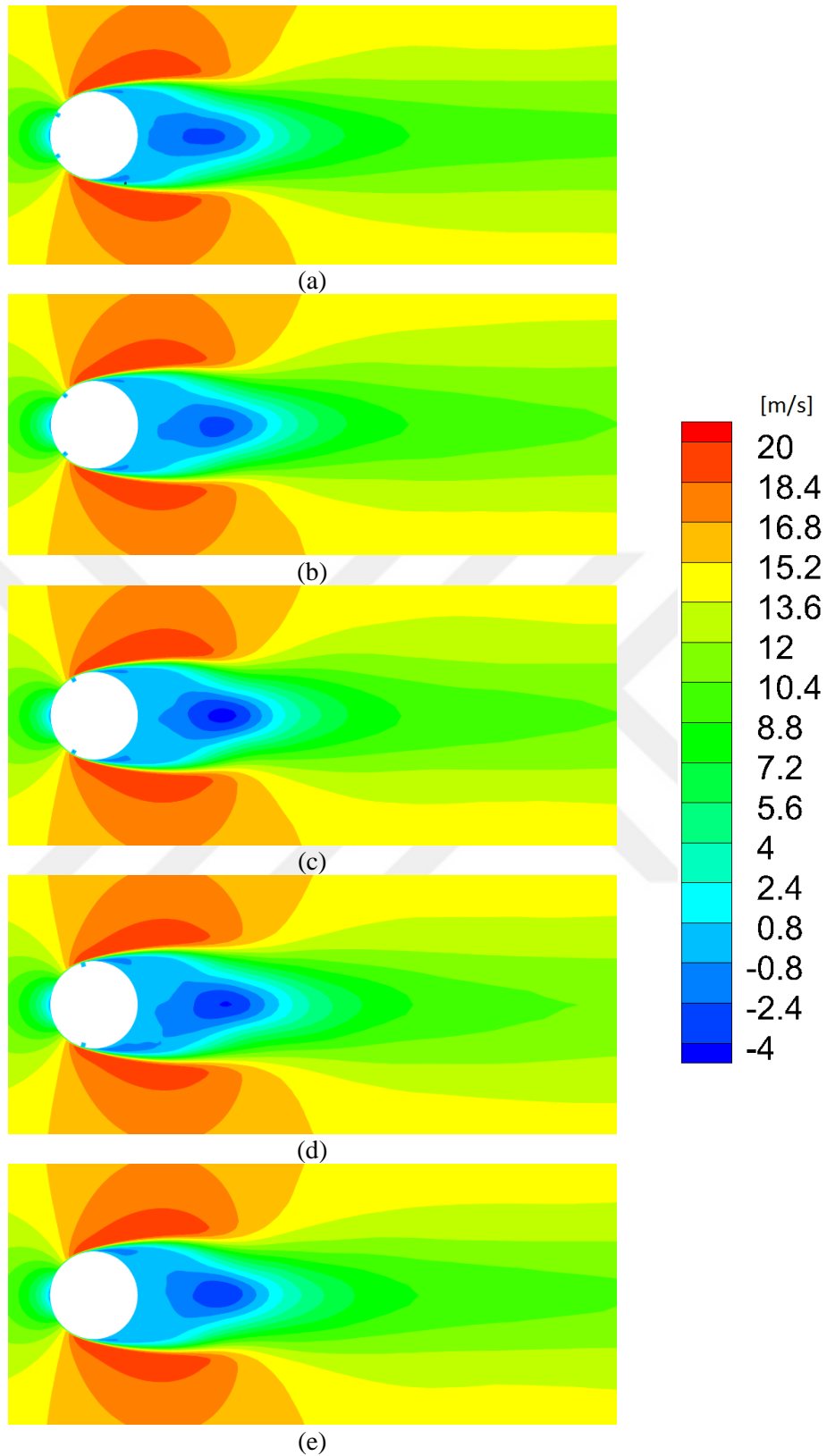


(e)

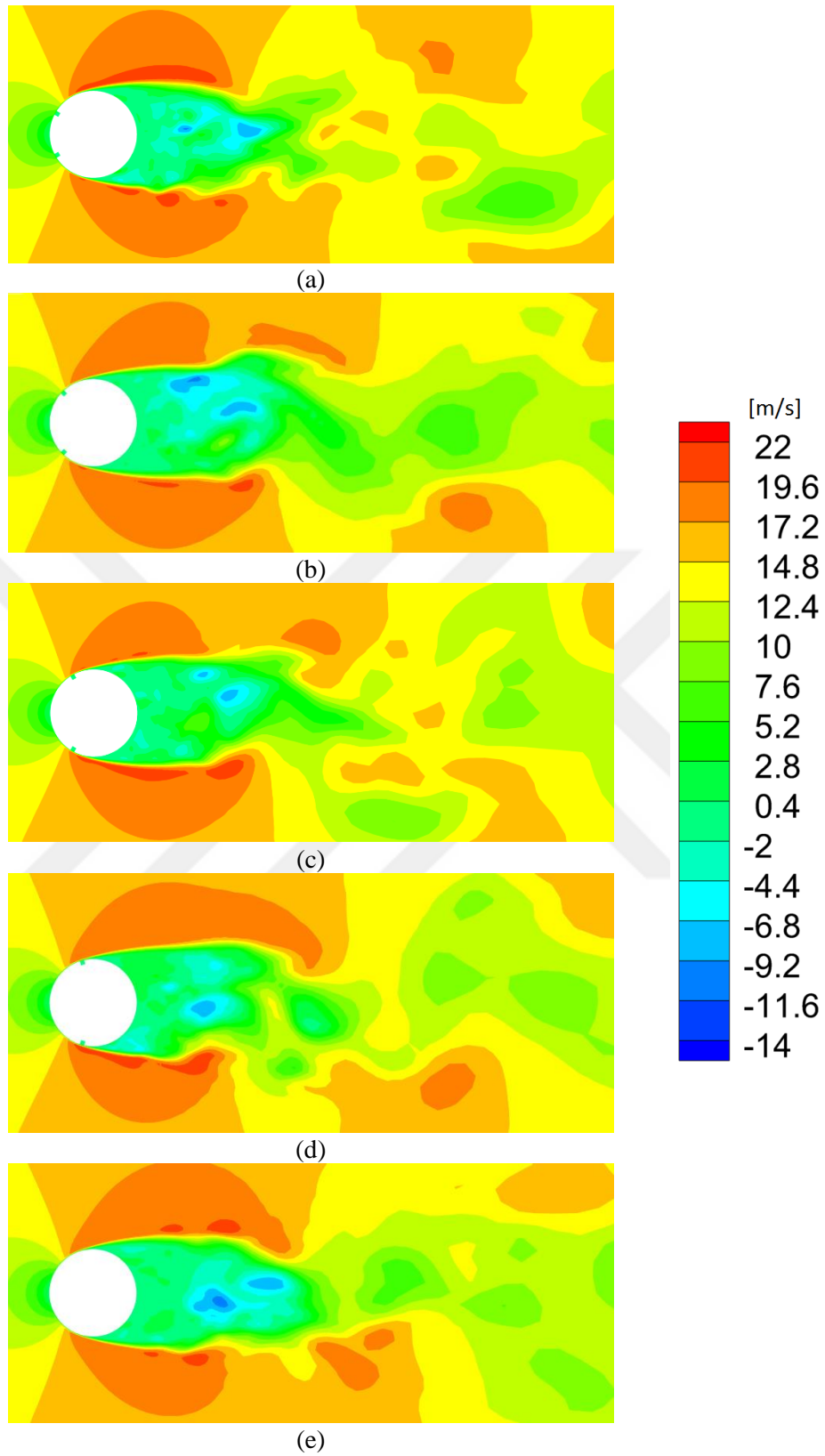
**Figure 4.8** The time-averaged streamlines for (a) 0.05D - 30°, (b) 0.05D - 45°, (c) 0.05D - 60°, (d) 0.05D - 75° and (e) bare circular cylinder



**Figure 4.9** The instantaneous streamlines for (a)  $0.05D - 30^\circ$ , (b)  $0.05D - 45^\circ$ , (c)  $0.05D - 60^\circ$ , (d)  $0.05D - 75^\circ$  and (e) bare circular cylinder



**Figure 4.10** The mean x velocity contour for (a) 0.05D - 30°, (b) 0.05D - 45°, (c) 0.05D - 60°, (d) 0.05D - 75° and (e) bare circular cylinder



**Figure 4.11** The instantaneous x velocity contour for (a) 0.05D - 30°, (b) 0.05D - 45°, (c) 0.05D - 60°, (d) 0.05D - 75° and (e) bare circular cylinder

### 4.3 Analysis of drag, $C_{lrms}$ and Strouhal number for 0.1D

In this section, we will discuss the simulation for 0.1D grooves size cylinder. The angular position of the groove was changed four times, which the angular positions were taken  $30^\circ$ ,  $45^\circ$ ,  $60^\circ$  and  $75^\circ$  relative to the forward stagnation point. The grooves were square-shaped and taken 10% of the cylinder diameters.

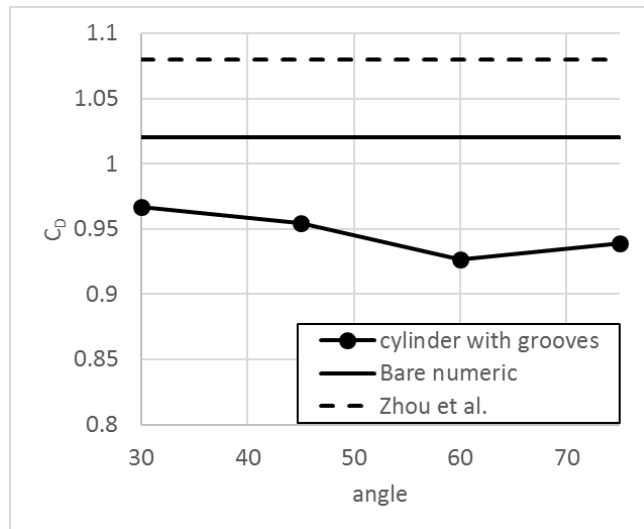
As shown in the table 4.5, drag coefficient, Strouhal number and R.M.S of lift coefficient for different angular position grooves cylinder were compared with bare cylinder. It can be seen as in table 4.5 Strouhal number has not changed with  $30^\circ$ -0.1D and  $45^\circ$ -0.1D angular position while it has slightly increased with  $60^\circ$ - 0.1D and  $75^\circ$ -0.1D grooved cylinders. That is shown, 0.1 D size of grooves generally have not affected unsteadiness of the flow behind a cylinder.

**Table 4.5** Strouhal number, drag coefficient and R.M.S of lift coefficient values for bare cylinder and different angular positions of grooves cylinder

Case	St	$C_d$	$C_{lrms}$
0.1D - $30^\circ$	0.209	0.96	0.128
0.1D - $45^\circ$	0.209	0.95	0.090
0.1D - $60^\circ$	0.214	0.92	0.084
0.1D - $75^\circ$	0.214	0.93	0.117
Bare cylinder	0.209	1.02	0.139

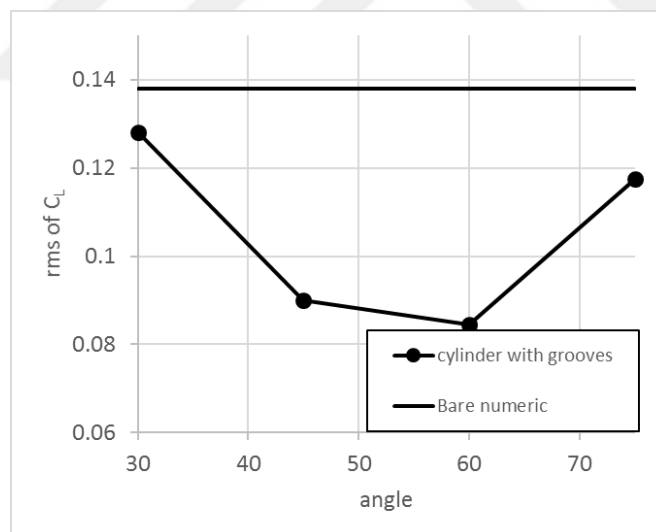
The drag coefficient for  $30^\circ$ ,  $45^\circ$ ,  $60^\circ$  and  $75^\circ$  angular position grooved cylinder is lower than bare cylinder. The drag coefficient for all cases decreased compared to bare cylinder. Maximum reduction of drag coefficient has observed at  $60^\circ$  as nearly %10. The drag coefficient has predicted 0.96, 0.95, 0.92, and 0.93 for  $30^\circ$ -0.1D,  $45^\circ$ -0.1D,  $60^\circ$ -0.1D and  $75^\circ$ - 0.1D, respectively. Variation of drag coefficient with angular positions for 0.1D are presented figure 4.12.





**Figure 4.12** Variation of drag coefficient with angular positions for 0.1D

The variation of R.M.S. of lift coefficient with angles for 0.1D is presented Figure 4.1. The  $C_{lrms}$  is smaller than bare cylinder for all cases of 0.1D. Using two grooves of 0.1D size is well suited for reduction of  $C_{lrms}$ . The maximum reduction of  $C_{lrms}$  has observed at 60 degree as nearly %40. The reduction of  $C_{lrms}$  has predicted %7, %35, %15 for 30°-0.1D, 45°-0.1D, and 75°- 0.1D, respectively.



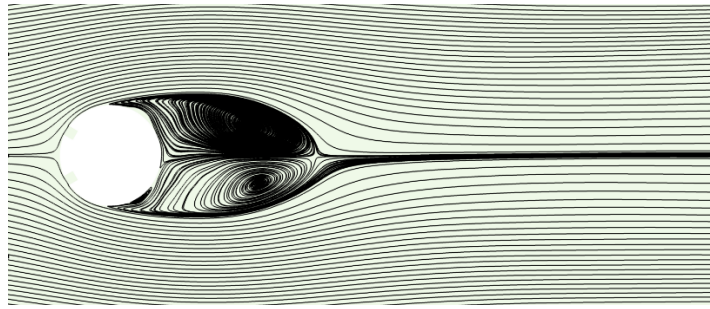
**Figure 4.13** Variation of R.M.S. of lift coefficient with angles for 0.1D.

Figure 4.14 presents the time-averaged streamlines for (a) 0.1D - 30°, (b) 0.1D - 45°, (c) 0.1D - 60°, (d) 0.1D - 75° and (e) bare circular cylinder. For better comparison, the nondimensional stream function has been used, the minimum and maximum nondimensional stream function values are “0” and “1”, respectively. The step size between streamlines is 0.004. After the cylinder, the recirculation zone and primary eddy is shown clearly for all cases. The length of  $L_R$ ,  $a$  and  $b$  are given at Table 4.6 for all cases of 0.1D. Figure 4.15 presents the instantaneous streamlines for (a) 0.1D - 30°, (b) 0.1D - 45°, (c) 0.1D - 60°, (d) 0.1D - 75° and (e) bare circular cylinder. The instantaneous velocity distributions are not symmetric for all cases.

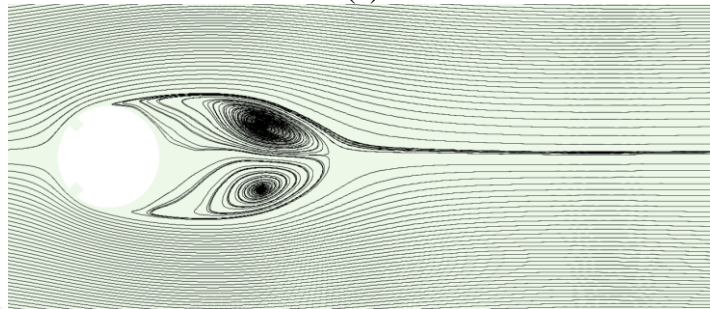
**Table 4.6** The length of  $L_R$ ,  $a$  and  $b$  for 0.1D

Case	$L_R$	$a$	$B$
0.1D- 30°	2.14D	1.5D	0.56D
0.1D- 45°	2.15D	1.48D	0.55D
0.1D- 60°	2.22D	1.44D	0.60D
0.1D- 75°	1.93D	1.33D	0.55D
Bare cylinder	1.98D	1.34D	0.55D

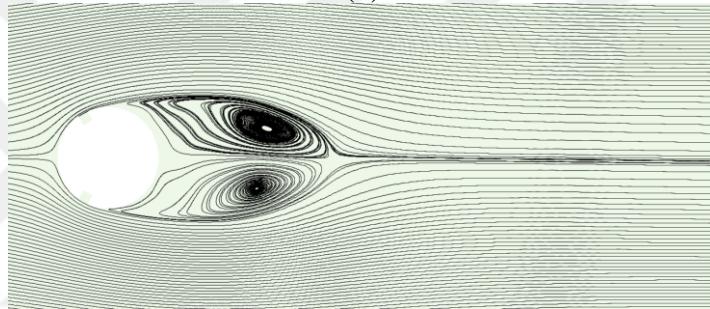
Figure 4.16 shows the time-averaged x-velocity distributions for (a) 0.1D - 30°, (b) 0.1D - 45°, (c) 0.1D - 60°, (d) 0.1D - 75° and (e) bare circular cylinder. The time of  $200D/U$  is taken for averaging of time. The recirculation zone is observed after the cylinders, whereas the maximum velocities are acquired at top of and the bottom the cylinder for all cases. Length of recirculation zone is important parameter for understanding flow mechanism. Figure 4.17 shows the instantaneous x velocity contour for (a) 0.1D - 30°, (b) 0.1D - 45°, (c) 0.1D - 60°, (d) 0.1D - 75° and (e) bare circular cylinder. The instantaneous velocity distributions are not enough to have knowledge about flow structure, whereas the maximum velocities are acquired at top of and the bottom the cylinder for all cases.



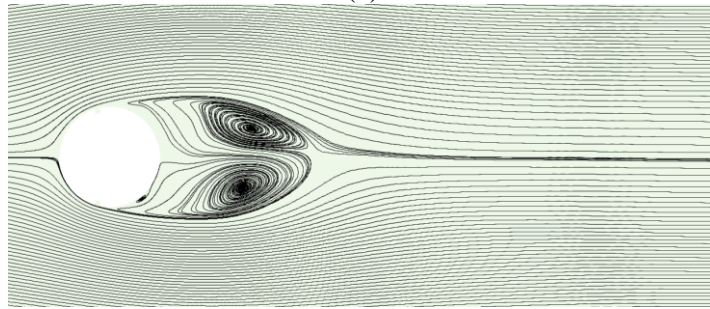
(a)



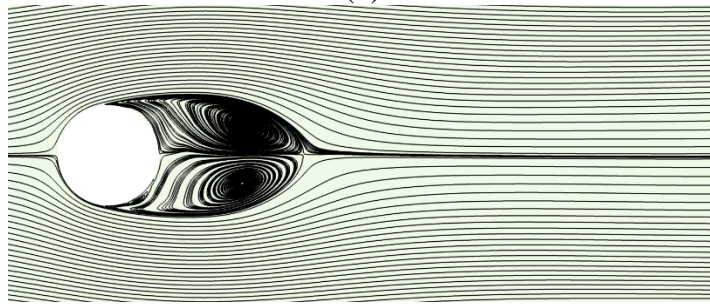
(b)



(c)

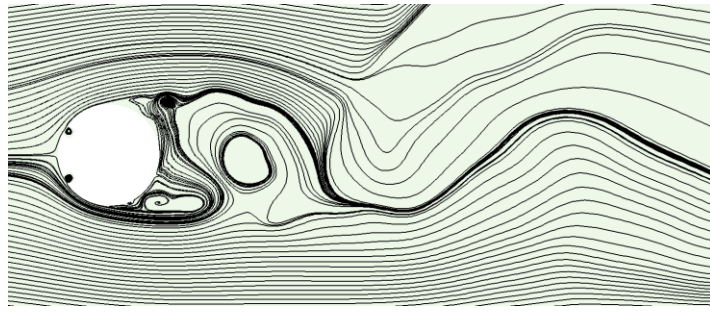


(d)

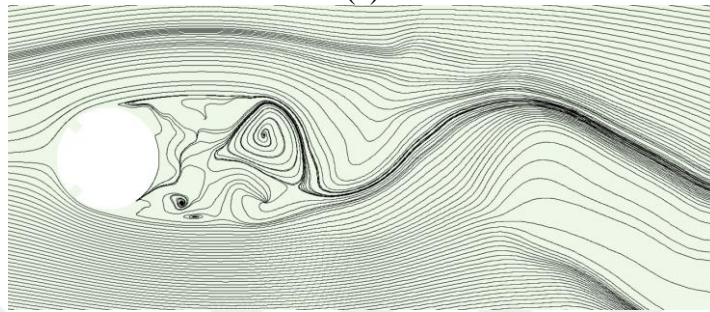


(e)

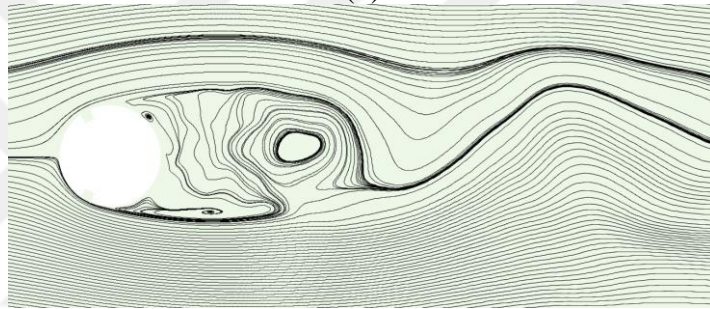
**Figure 4.14** The time-averaged streamlines for (a) 0.1D - 30°, (b) 0.1D - 45°, (c) 0.1D - 60°, (d) 0.1D - 75° and (e) bare circular cylinder



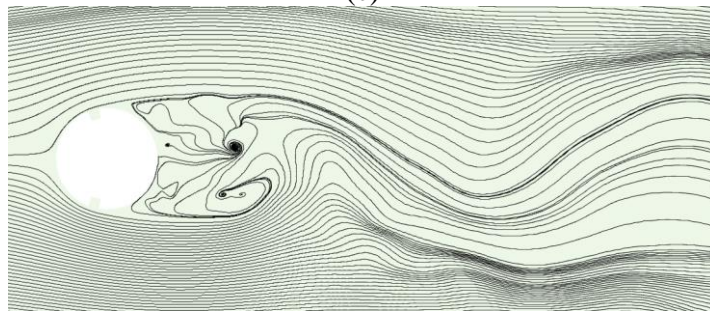
(a)



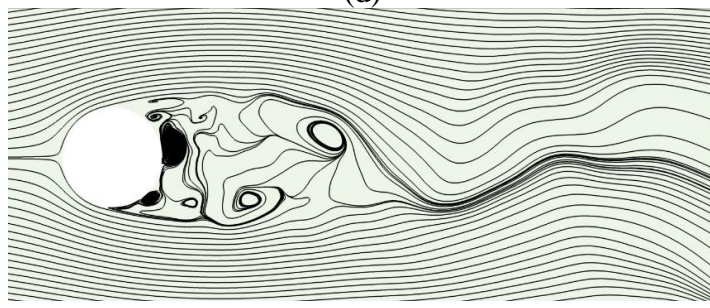
(b)



(c)

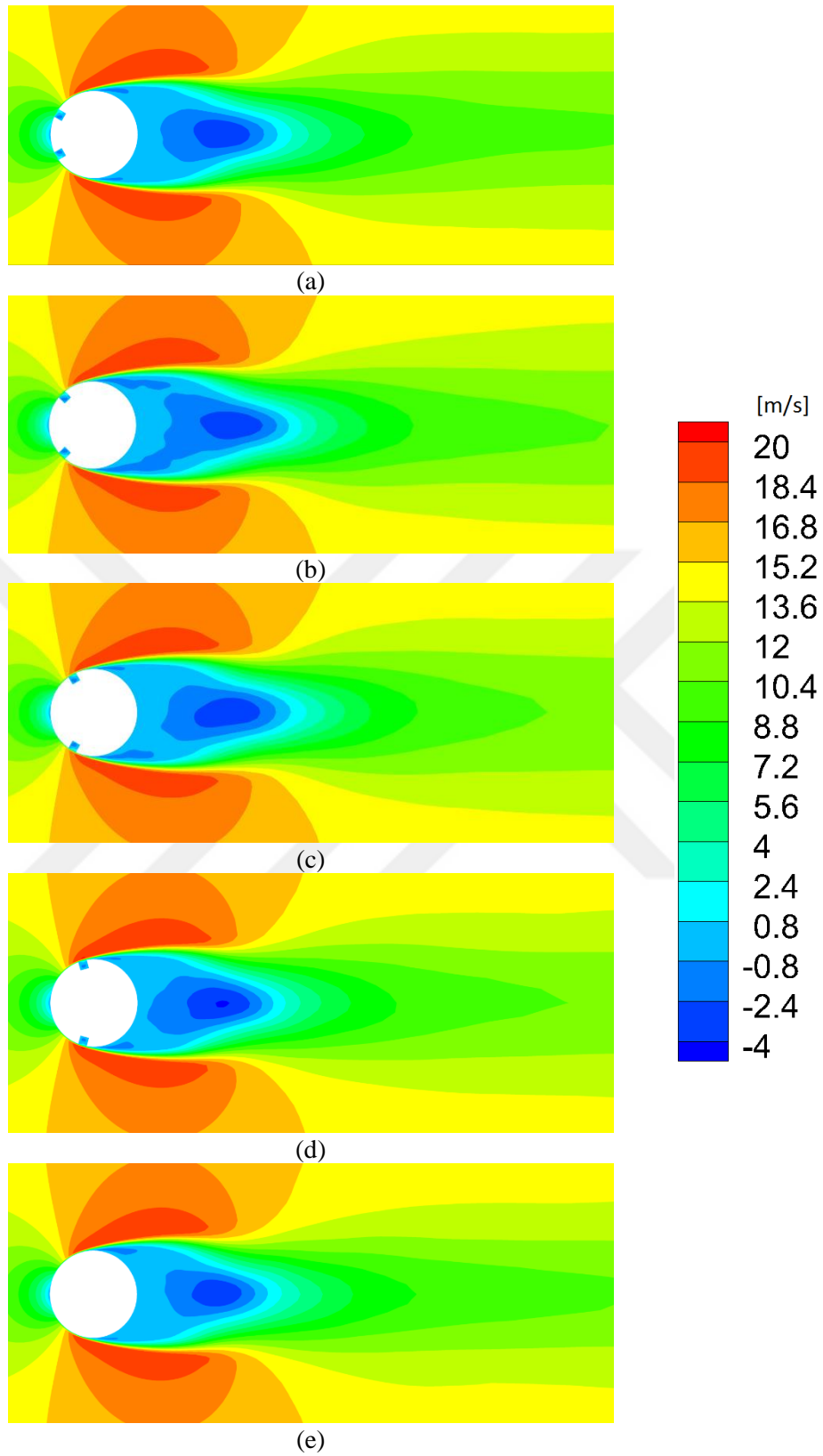


(d)

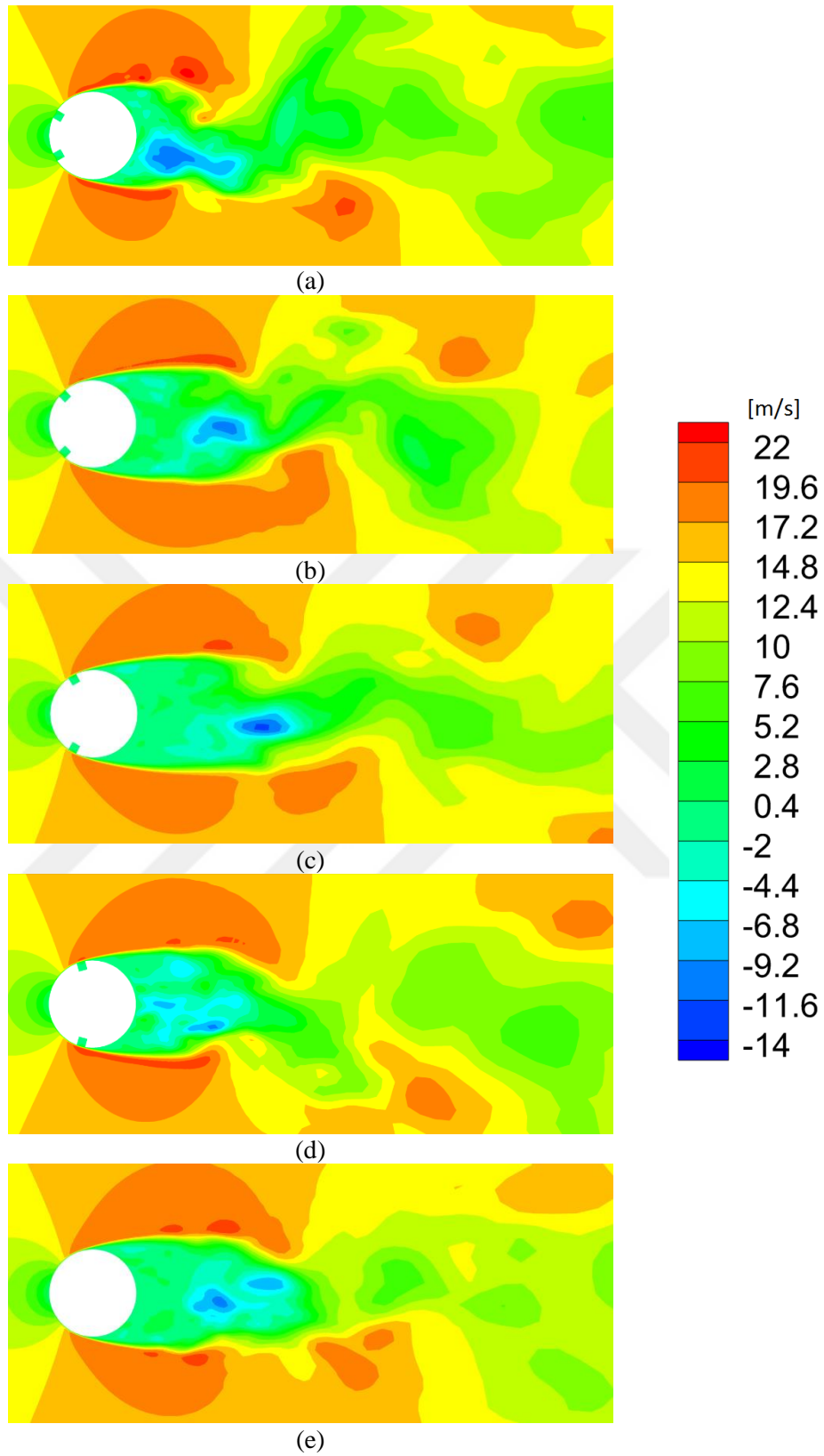


(e)

**Figure 4.15** The instantaneous streamlines for (a)  $0.1D - 30^\circ$ , (b)  $0.1D - 45^\circ$ , (c)  $0.1D - 60^\circ$ , (d)  $0.1D - 75^\circ$  and (e) bare circular cylinder



**Figure 4.16** The mean x velocity contour for (a) 0.1D - 30°, (b) 0.1D - 45°, (c) 0.1D - 60°, (d) 0.1D - 75° and (e) bare circular cylinder



**Figure 4.17** The instantaneous x velocity contour for (a) 0.1D - 30°, (b) 0.1D - 45°, (c) 0.1D - 60°, (d) 0.1D - 75° and (e) bare circular cylinder

#### 4.4 Analysis of drag, $C_{lrms}$ and Strouhal number for 0.15D

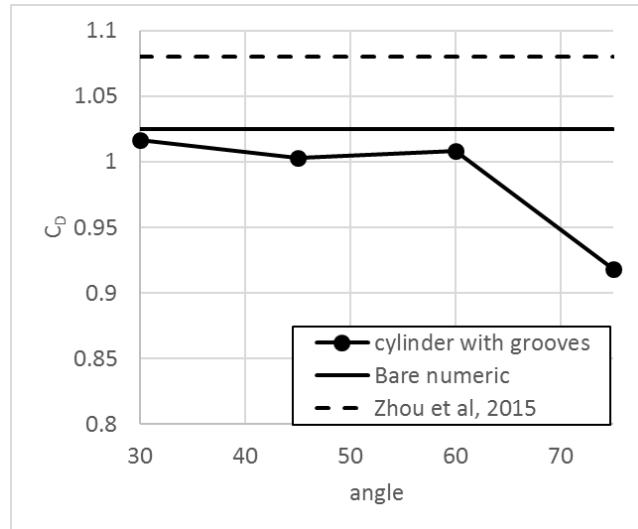
In this section, we will discuss the simulation for 0.15D grooves size cylinder. The angular position of the groove was changed four times, which the angular positions were taken  $30^\circ$ ,  $45^\circ$ ,  $60^\circ$  and  $75^\circ$  relative to the forward stagnation point. The grooves were square-shaped and taken 15% of the cylinder diameters.

As it is presented in the table 4.7, drag coefficient, Strouhal number and R.M.S of lift coefficient for different angular position grooves cylinder were compared with bare cylinder. It can be seen as in table 4.7 Strouhal number generally has not changed with angular position. Strouhal number is slightly higher than bare cylinder for  $75^\circ$  and 0.15D. That is shown, 0.15 D size of grooves generally have not affected unsteadiness of the flow behind a circular cylinder.

**Table 4.7** Strouhal number, drag coefficient and R.M.S of lift coefficient values for bare cylinder and different angular positions of grooves cylinder

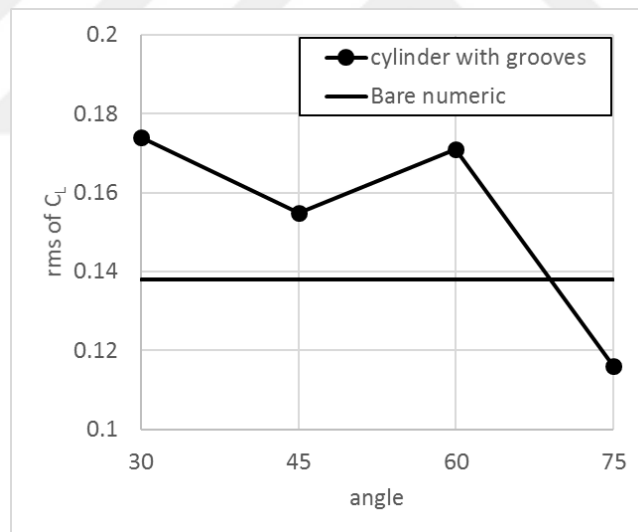
Case	St	$C_d$	$C_{lrms}$
$30^\circ$	0.209	1.017	0.174
$45^\circ$	0.209	1.003	0.155
$60^\circ$	0.209	1.008	0.171
$75^\circ$	0.219	0.917	0.116
Bare cylinder	0.209	1.02	0.139

The drag coefficient for  $30^\circ$ ,  $45^\circ$ ,  $60^\circ$  and  $75^\circ$  angular position grooved cylinder is lower than bare cylinder. The drag coefficient for all cases decreased compared to bare cylinder. Maximum reduction of drag coefficient has observed at 75 degree as nearly %11. The drag coefficient has predicted 1.017, 1.003, 1.008, and 0.917 for  $30^\circ$ -0.15D,  $45^\circ$ -0.15D,  $60^\circ$ -0.15D and  $75^\circ$ - 0.15D, respectively. Variation of drag coefficient with angular positions for 0.15D are presented figure 4.18.



**Figure 4.18** Variation of drag coefficient with angles for 0.15D

Figure 4.19 shows the variation of R.M.S of lift coefficient with angles for 0.15D. The rms of lift coefficient is smaller than bare cylinder for 0.15D-75°. The R.M.S of lift coefficient is higher than bare cylinder for other cases of 0.15D. The maximum reduction of R.M.S of lift coefficient lift has observed at 75° as nearly %12.



**Figure 4.19** Variation of R.M.S of lift coefficient with angles for 0.15D.

Figure 4.20 presents the time-averaged streamlines for (a) 0.15D - 30°, (b) 0.15D - 45°, (c) 0.15D - 60°, (d) 0.15D - 75° and (e) bare circular cylinder. For better comparison, the nondimensional stream function has been used, the minimum and maximum nondimensional stream function values are “0” and “1”, respectively. The step size between streamlines is 0.004. After the cylinder, the recirculation zone and primary eddy is shown clearly for all cases. The length of  $L_R$ ,  $a$  and  $b$  are given at Table 4.8 for all cases of 0.15D. Figure 4.15 presents the instantaneous streamlines for (a)

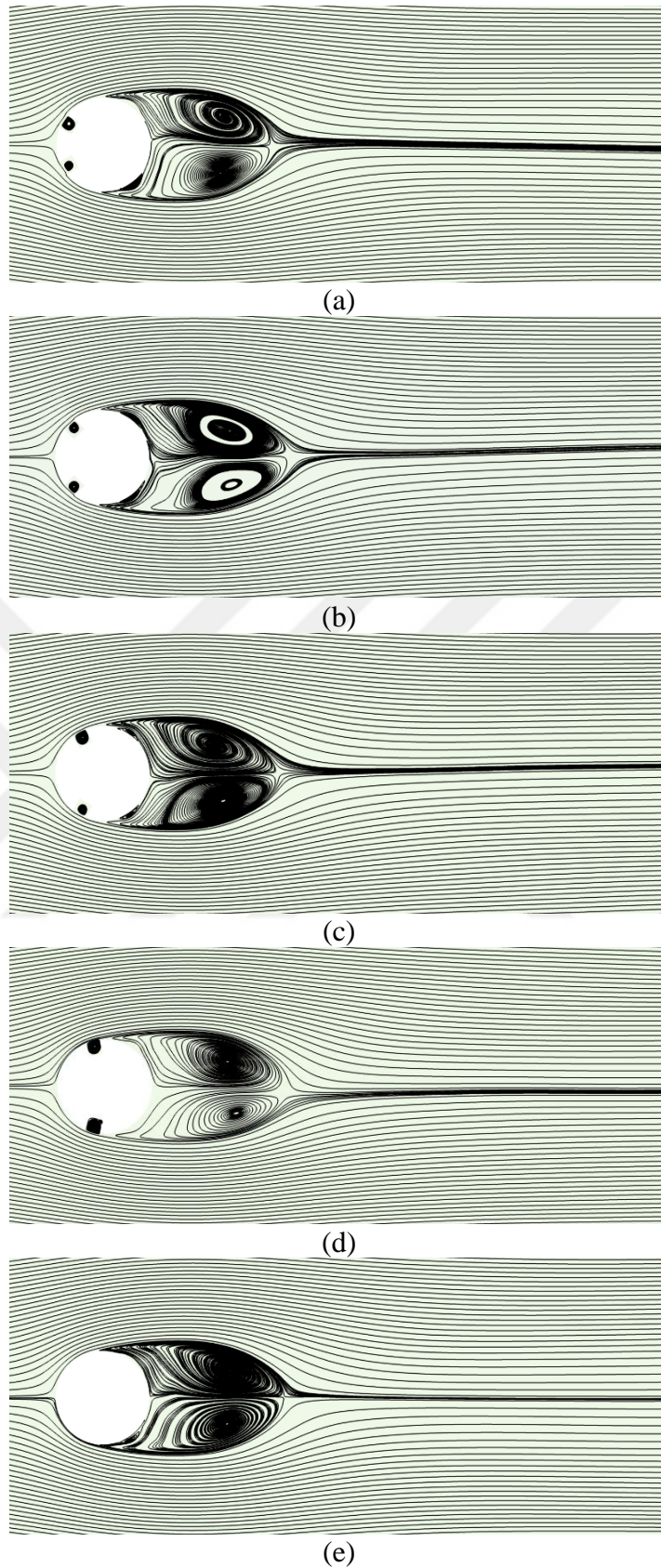


0.15D - 30°, (b) 0.15D - 45°, (c) 0.15D - 60°, (d) 0.15D - 75° and (e) bare circular cylinder. The instantaneous velocity distributions are not symmetric for all cases.

**Table 4.8** The length of  $L_R$ ,  $a$  and  $b$  for 0.15D

Case	$L_R$	$a$	$B$
0.15D- 30°	2.03D	1.24D	0.57D
0.15D- 45°	2.00D	1.36D	0.57D
0.15D- 60°	2.06D	1.28D	0.59D
0.15D- 75°	2.01D	1.38D	0.53D
Bare cylinder	1.98D	1.34D	0.55D

Figure 4.22 shows the time-averaged x-velocity distributions for (a) 0.15D - 30°, (b) 0.15D - 45°, (c) 0.15D - 60°, (d) 0.15D - 75° and (e) bare circular cylinder. The time of  $200D/U$  is taken for averaging of time. The recirculation zone is observed after the cylinders, whereas the maximum velocities are acquired at top of and the bottom the cylinder for all cases. Length of recirculation zone is important parameter for understanding flow mechanism. Figure 4.23 shows the instantaneous x velocity contour for (a) 0.15D - 30°, (b) 0.15D - 45°, (c) 0.15D - 60°, (d) 0.15D - 75° and (e) bare circular cylinder. The instantaneous velocity distributions are not enough to have knowledge about flow structure, whereas the maximum velocities are acquired at top of and the bottom the cylinder for all cases.



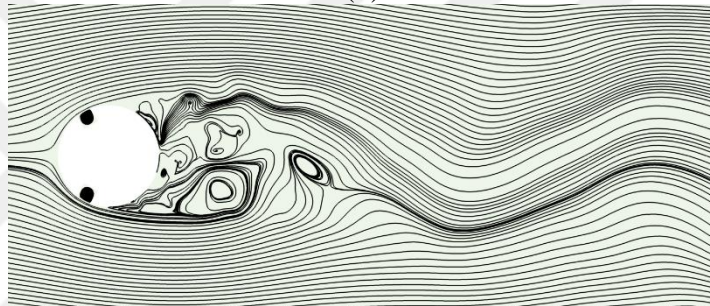
**Figure 4.20** The time-averaged streamlines for (a)  $0.15D - 30^\circ$ , (b)  $0.15D - 45^\circ$ , (c)  $0.15D - 60^\circ$ , (d)  $0.15D - 75^\circ$  and (e) bare circular cylinder



(a)



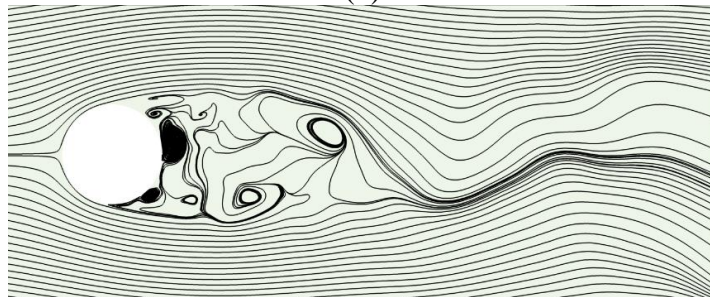
(b)



(c)

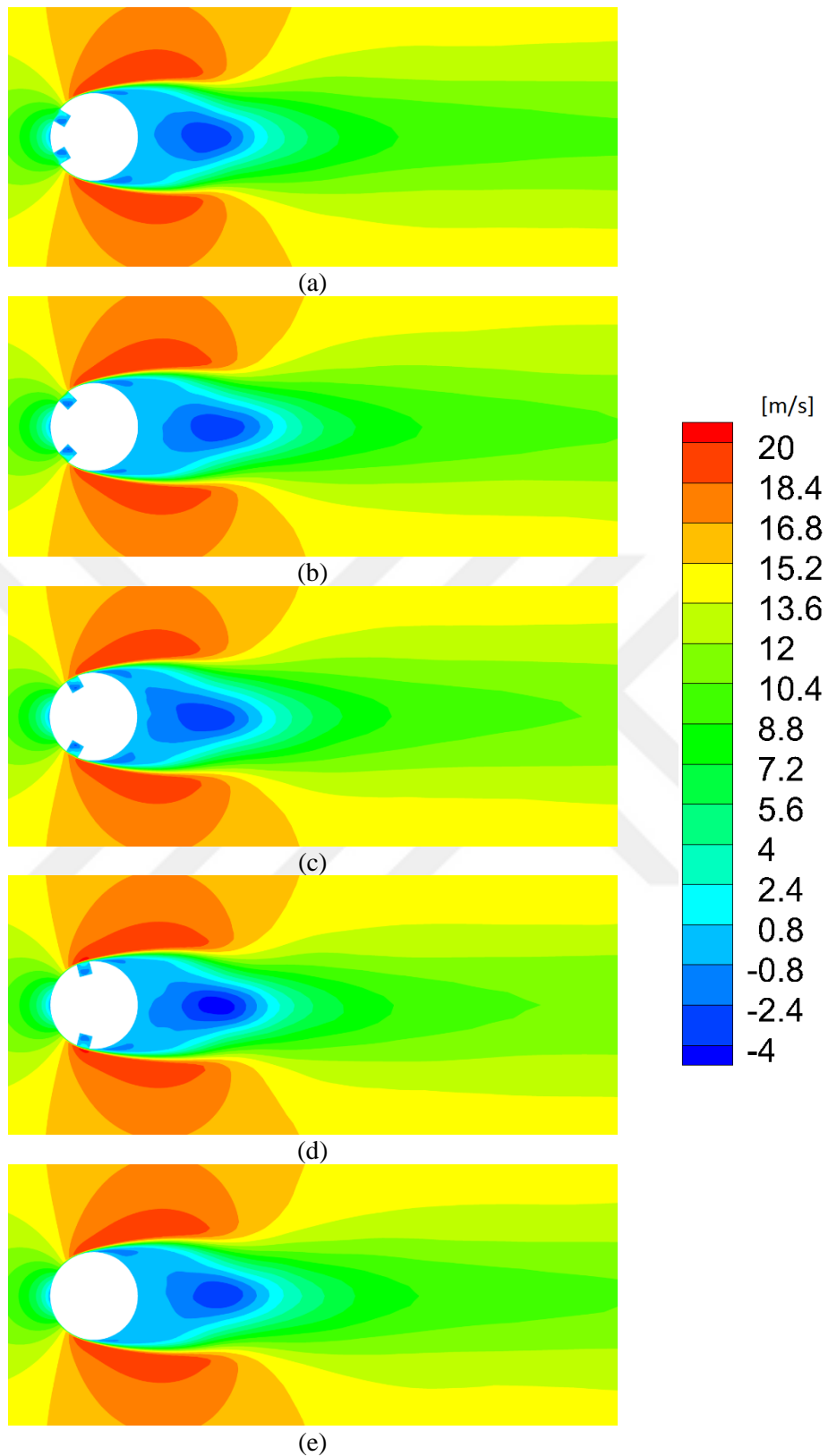


(d)

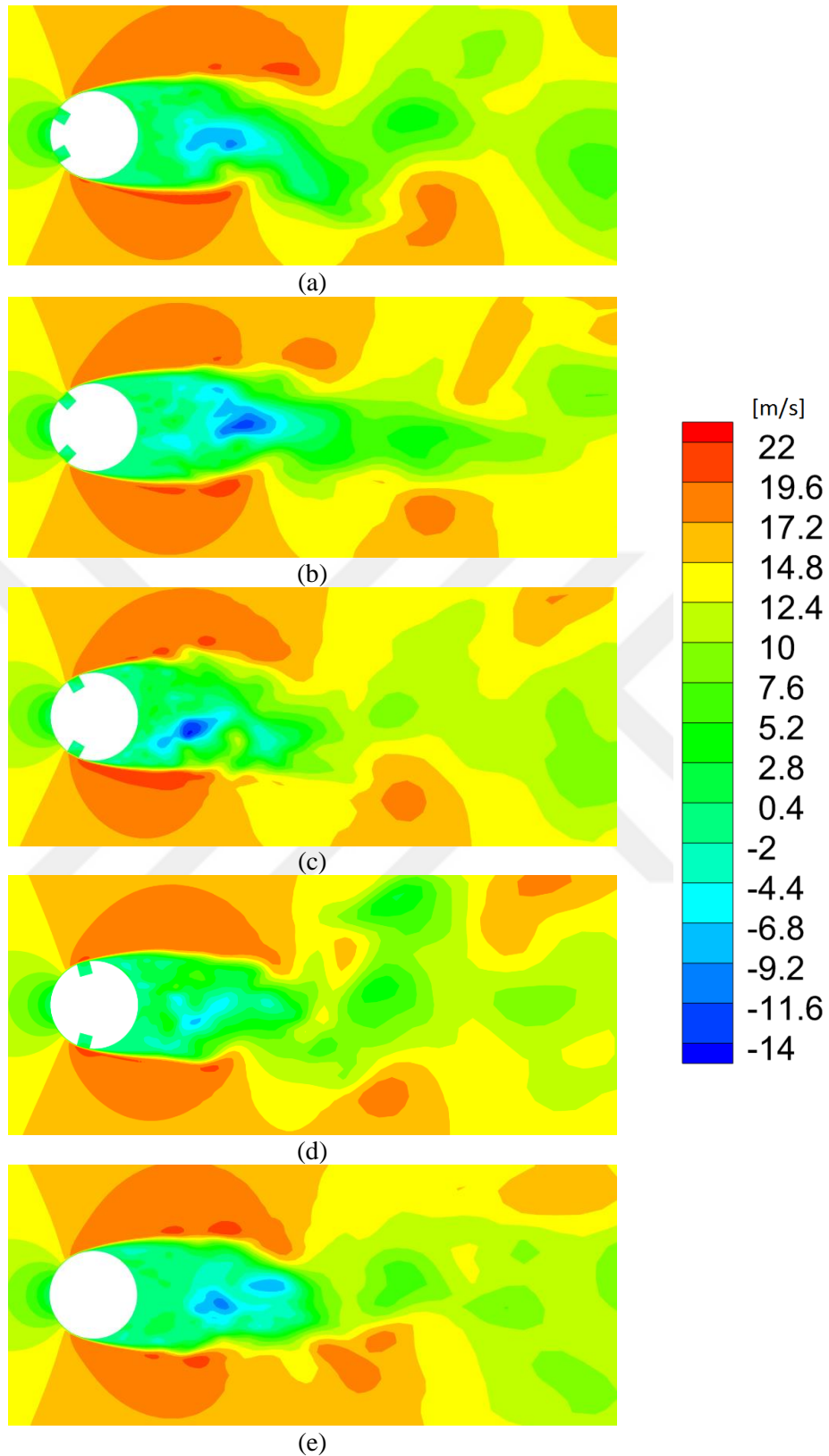


(e)

**Figure 4.21** The instantaneous streamlines for (a) 0.15D - 30°, (b) 0.15D - 45°, (c) 0.15D - 60°, (d) 0.15D - 75° and (e) bare circular cylinder



**Figure 4.22** The mean x velocity contour for (a) 0.15D - 30°, (b) 0.15D - 45°, (c) 0.15D - 60°, (d) 0.15D - 75° and (e) bare circular cylinder



**Figure 4.23** The instantaneous x velocity contour for (a) 0.15D - 30°, (b) 0.15D - 45°, (c) 0.15D - 60°, (d) 0.15D - 75° and (e) bare circular cylinder

## CHAPTER 5

### CONCLUSION

Investigation of recirculation length, drag coefficient, R.M.S of lift coefficient and Strouhal number is done numerically for bare cylinder and cylinder with two grooves for  $Re=10000$  with using finite volume method based on commercial code Ansys-Fluent. LES with Smagorinsky-Lilly model is applied for turbulence modelling. Three different grooves size which are  $0.05D$ ,  $0.1D$  and  $0.15D$  are used.  $30^\circ$ ,  $45^\circ$ ,  $60^\circ$  and  $75^\circ$  are defined as angular positions for two grooves. The main conclusions are drawn as follows:

- The maximum reduction rate for drag coefficient was from %10 to %11 which are observed at  $0.15D-75^\circ$  and  $0.1D - 60^\circ$ , respectively.
- Using two grooves was more suitable course for decreasing drag comparing to bare cylinder.
- Clrms decreased for all cases of  $0.1D$  and the maximum reduction rate of Clrms was nearly %40 less comparing to bare cylinder at  $0.1D-60^\circ$ .
- Strouhal number didn't change with angular position for all cases of groove sizes except for  $0.15D-75^\circ$ ,  $0.1D-60^\circ$  and  $0.1D-75^\circ$  which are slightly higher than bare cylinder.
- Strouhal number did not change with angular position for all cases of  $0.05D$ . Additionally, it was shown that the width of grooves did not affect the unsteadiness of the flow past a cylinder.
- Minimum length of recirculation zone is observed are  $0.05D - 45^\circ$ , whereas for  $0.1D - 60^\circ$ , the maximum length of recirculation zone is acquired

- In all numerical analysis, it was found that RMS of lift coefficient generally greater than the bare cylinder for 0.05D and 0.15D, but it was small for 0.1D compared to bare cylinder.



## REFERENCES

- Ansys. Ansys Fluent Theory Guide. ANSYS Inc., 13 editions,
- Batchelor G.K. (1967) *An Introduction to Fluid Dynamics*. Cambridge University Press
- Benim, A. C., Pasqualotto, E., Suh, S.H. (2008). Modelling turbulent flow past a circular cylinder by RANS, URANS, LES and DES. *Prog. Compt. Fluid Dynamics* **8(5)**, 299-307.
- Bloor, M.S. (1964). The transition to turbulence in the wake of a circular cylinder. *Journal of Fluid Mechanics*, **19**, 290-304.
- Bou, Z., Xikun, W., Wei, G., Jiabin, Z., Soon, K.T. (2015). 'Experimental measurements of the drag force and the near-wake flow patterns of a longitudinally grooved cylinder' *Journal of Wing Engineering and Industrial Aerodynamics* **145**, 30-41.
- Bou, Z., Xikun, W., Wei, G., Jiabin, Z., Soon, K.T. (2015). 'Experimental study on flow past a circular cylinder with rough surface' *Journal of Ocean Engineering* **109**, 7-13
- Canpolat, C. (2015). Characteristics of flow past a circular cylinder with a rectangular groove. *Flow Measurement Instrumentation* **45**, 233-246.
- Canpolat, C., Sahin, B. (2017). Influence of single rectangular groove on the flow past a circular cylinder. *Int. J. Heat Fluid Flow* **64**, 79-88
- Ching, J. C., Shenq-Yuh, J. (1998). *Fundamentals of turbulence modeling*, Taylor & Francis
- Dong, S., Karniadakis G. E. (2005). DNS of flow past a stationary and oscillating cylinder at  $Re=10000$ . *J. Fluids Structures* **20**, 519-531



Dyke, 1982; Album of fluid Motion, Parabolic Press, UK

Feng, L.H., Wang, J.J., (2010). Circular cylinder vortex-synchronization control with a synthetic jet positioned at the rear stagnation point, *Journal of Fluid Mechanics*, **662**, 232-259.

Ferziger, J. H., Perić, M. (1996). *Computational Methods for Fluid Dynamics*. Berlin etc., Springer-Verlag

Owen, J.C., Bearman, P.W., Szewczyk, A.A. (2001). Passive control of VIV with drag reduction, *Journal of Fluids and Structures*, **15**, 597-605.

Kai, L., Jianqiang, D., Mei, M. (2016). Experimental study on the confined flow over a circular cylinder with a splitter plate, *Flow Measurement and Instrumentation*, **51**, 95-104

Karabelas, S. J., Koumroglou, B. C., Argyropoulos, C.D., Markatos, N.C. (2012). High Reynolds number turbulent flow past a rotating cylinder, *Applied Mathematical Modelling* **36**, 379–398,

Lee, S.J., Lee, J. Y., (2008). PIV measurements of the wake behind a rotationally oscillating circular cylinder, *Journal of Fluids and Structures*, Republic of Korea, **24**, 2–17.

Muddada, S., Patnaik, B. S. V., (2009). An active flow control strategy for the suppression of vortex structures behind a circular cylinder, *European Journal of Mechanics B/Fluids*, India, **29**, 93–104

Norberg, C. (2003). Fluctuating lift on a circular cylinder: review and new measurements, *J. Fluids Structures* **17**, 57-96.

ROSHKO A. (1954). On the development of turbulent wakes from vortex streets. NACA Rep. 1191.

Kim S. J., Lee C.M. (2000). Investigation of the flow around a circular cylinder under the influence of an electromagnetic force, *Journal of Experiments in Fluids* **28(3)**, 252-260

Smagorinsky J. (1963). General circulation experiments with the primitive equations I: The basic experiment, *Monthly Weather Review* **91(3)**

- Sunghan, K., Philip, A., Wilson, Z. M. C. (2015). Large-eddy simulation of the turbulent near wake behind a circular cylinder: Reynolds number effect, *Applied Ocean Research* **49**, 1-8
- Sumer, B.M. and Fredsøe, J. (1997). Hydrodynamics around Cylindrical Structures, Advanced series on ocean engineering, **Vol. 12**, World Scientific, Singapore.
- Sumer, B.M. and Fredsøe, J. (1997). Flow around a cylinder in steady current, *Advanced Series on Ocean Engineering*.
- Williamson C. H. K. (1989). Oblique and parallel modes of vortex shedding in the wake of a circular cylinder at low Reynolds number, *J. Fluid Mech.*, **206**, 579-627
- Williamson C.H.K. (1988). The existence of two stages in the transition to three-dimensionality of a cylinder wake, *Phys. Fluids*, **31(11)**, 3165-316
- Wu, W., Yuan, J., Cheng, L. (2007). Multi-high-frequency perturbation effects on flow-induced vibration control, *Journal of Sound and Vibration*, Hong Kong, **305**, 226–242.
- Zhang, H., Yang J. M., Xiao, L.F., Lü, H.N. (2015). Large eddy simulation of flow past both finite and infinite circular cylinders at  $Re = 3900$ , *Journal of Hydrodynamics* **27(2)**, 195-203